Geotech Geol Eng
https://doi.org/10.1007/s10706-024-02770-z

ORIGINAL PAPER

Physical, Chemical and Compaction Characteristics of Slightly Weathered Tephras of New Zealand

Shaurya Sood · Gabriele Chiaro · Thomas Wilson · Mark Stringer

Received: 5 September 2023 / Accepted: 9 February 2024
© The Author(s) 2024

Abstract The North Island of New Zealand is a region of high volcanic activity, with significant eruptions over the past. Analogous to past events, future volcanic eruptions would produce a considerable volume of ash and granular soils, covering widespread areas and raising concerns for their disposal and storage. Such deposits, primarily airfall tephra, could be potentially used in geotechnical engineering applications such as foundations, roadway embankments and land reclamations. However, before their use as structural fills can be recommended, detailed laboratory investigations of their physical, chemical, compaction, and geotechnical engineering properties (strength, compressibility, collapsibility, liquefaction potential, etc.) must be conducted. Different tephra deposits can be products of different eruptions, so chemical composition analyses can be combined with the physical, compaction, and engineering properties to characterize such deposits. Accordingly, this paper provides useful insights from physical (grain size, specific gravity, and morphology), chemical (elemental and mineralogy using X-ray fluorescence and X-ray diffraction), and compaction tests (maximum dry density, optimum water content, and particle breakage) for eleven selected volcanic tephra samples sourced from the North Island of New Zealand in the Rotorua, Taupo, and Auckland regions.

Keywords Tephras · Chemical composition · Physical properties · Compaction · Particle breakage

S. Sood (✉) · G. Chiaro · M. Stringer
Department of Civil and Natural Resources Engineering, University of Canterbury, Christchurch 8041, New Zealand
e-mail: shaurya.sood@pg.canterbury.ac.nz

G. Chiaro
e-mail: gabriele.chiaro@canterbury.ac.nz

M. Stringer
e-mail: mark.stringer@canterbury.ac.nz

T. Wilson
Department of Earth and Environment, University of Canterbury, Christchurch 8041, New Zealand
e-mail: thomas.wilson@canterbury.ac.nz

1 Introduction

New Zealand (NZ) is an island country in the southwestern Pacific Ocean comprising two major land masses—the North Island and the South Island. The primary volcanic activity is concentrated in the North Island, which runs from Bay of Islands, Auckland (Auckland Volcanic Field AVF), Rotorua–Taupo (Taupo Volcanic Zone TVZ), and Taranaki/Egmont E (Lowe and Balks, 2019). While the high activity of TVZ is subduction-driven, the lesser activity of AVF is due to feeding from a magmatic region. The central North Island, particularly TVZ, has witnessed the biggest eruptions in this country—the most destructive NZ eruption of recent times being Mount Tarawera in 1886. On the other hand, the AVF, covering much of the metropolitan area of Auckland, includes

Published online: 09 March 2024

existing 53 monogenetic volcanic centers but the field is still active (Lindsay et al. 2011).

Tephra refers to the solid constituent contained in volcanic gas in an explosive volcanic eruption. It can be broadly classified into two groups—'tephra fall deposit' and 'pyroclastic flow deposit'. The tephra fall deposit is the depositing product of the volcanic ash and pumice carried on in the wind during the Plinian (explosive column rising over the volcano) eruption. As the volcanic deposits constitute a variety of grain sizes and densities, they fall at relative distances from the volcano. Hence, the tephra fall deposits usually have a uniform grain size distribution. In contrast, the pyroclastic flow deposit is provided by the volcanic column containing pumice, volcanic ash, and scoria yielding to gravity action and further flowing above the ground. These kinds of deposits—'tephra airfall' and 'pyroclastic flow' deposits—are abundantly found in Rotorua and Auckland regions due to the high volcanism observed in these regions. For a city such as Auckland, which is home to 1.5 million people, the management of such deposits becomes even more critical to restore the functionality of the area in case of an eruption (Hayes et al. 2017).

Many of today's TVZ and AVF soils comprise weathered tephra materials that originated from previous airfall events; with future eruptions tending to produce newer identical deposits. These would range from fine-grained ashes to granular scoria or pumice. Because of abundance and economic considerations, these airfall deposits have been used in the past and will be used in the future in geotechnical engineering applications, for example as structural backfills or land reclamation fills. However, understating their response when subjected to extreme rain and flood events due to climate change, and associated potential accelerated weathering processes in combination with earthquake conditions, is of paramount importance before their use as structural fills can be further recommended. To do so, detailed laboratory investigations of their physical, chemical, compaction, and geotechnical engineering properties (strength, compressibility, collapsibility, liquefaction potential, etc.) are necessary.

As also these volcanic deposits are products of different times and eruptions, these might differ based on their physical and chemical properties (Pathiranagei et al. 2023). Accordingly, this paper provides useful insights from physical (grain size, specific gravity, and morphology), chemical (elemental and mineralogy using X-ray fluorescence and X-ray diffraction), and compaction tests (maximum dry density, optimum water content, and particle breakage) for selected volcanic tephra samples sourced from the North Island of New Zealand in the Rotorua, Taupo and Auckland regions. As a part of a detailed laboratory investigation, relationships between physio–chemical and compaction parameters were first established, in this paper, as they provide a preliminary direction for their selection as backfilling materials for geotechnical applications. The shear strength, one-dimensional compressibility, collapsibility due to water inundation, and liquefaction potential of such materials have been also assessed; their correlations with the physio–chemical and compaction properties will be presented in due course in companion papers by the authors focusing on detailed geotechnical aspects of compacted tephras.

2 Geological Background and Sampled Tephras

This study focuses on the physical, chemical, and compaction properties of 'recent', 'young', and 'older' tephras formed approximately 135, 705, and 140 ka years ago in the TVZ region along with 'older' depositions dating back to 200–260 ka and 35–180 ka years in the AVF. The TVZ is a volcanic zone in the North Island of New Zealand and has been highly active for the past 2 Ma. It runs offshore from the Bay of Plenty in the north to Mt. Ruapehu in the south (Fig. 1) including the most productive calderas in the world—Okataina and Taupo (Lowe 1990). The AVF, on the other hand, is a small-volume volcanic field within New Zealand's largest city, Auckland. Considering different geological sites, eruption times and possible weathering effects, the differences between the sampled tephras, thus, need thorough investigation.

The tephras under consideration in this study were from the following different eruptions: Tarawera 1886 and Kaharoa 1315 (Okataina caldera in TVZ), Taupo 140 ka (Taupo caldera in TVZ), Pupuke 200 ka and Maungataketake 85–200 ka (AVF). In NZ's geological history, the Tarawera and Kaharoa tephra samples come under very young (or recent) tephra and young tephra, respectively.

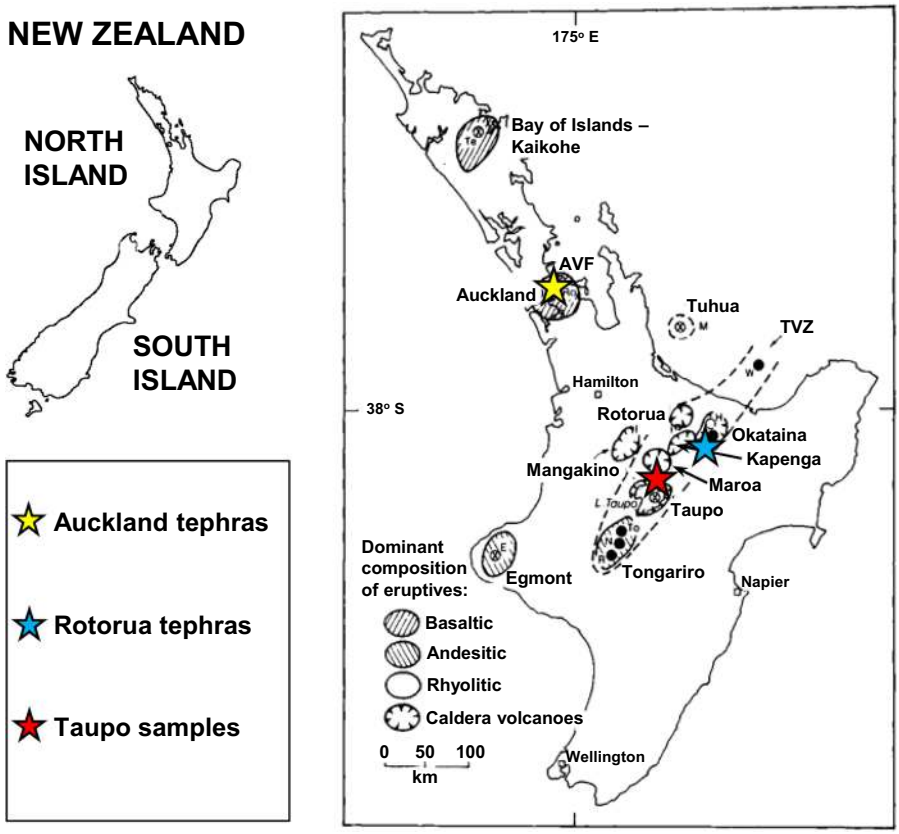

Fig. 1 Map showing TVZ comprising calderas and AVF containing volcanic centers with collective locations of sampled tephras (derived from Lowe 1990)

When a large quantity of tephra is deposited, the soil developed on it can be classified as a recent deposit such as Tarawera ash and lapilli, and Rotomahana mud from the 1886 'basaltic' eruption (Rijkse 1974). The 1315 Kaharoa eruption, instead, from Mt. Tarawera is the youngest 'rhyolitic' eruption and the largest in terms of volumetric deposition in the last millennium in NZ (Lowe and Balks 2019). The eruption triggered approximately 5 km^3 of rhyolitic deposits of block and ash flows to the north, southeast, and northwest of the volcano. The deposit namely, Kaharoa ash, was a coarse ash, with abundant blocks of pumiceous rhyolite, dacites, obsidian, and devitrified rhyolite. Blocks of granodiorite and granite were also found in them (Ewart and Cole 1967; Nairn et al. 2004). Nonetheless, the erupted products were mainly pyroclastic with a total volume of deposited materials of around 1 km^3 (Nairn 1979). In addition to the basaltic eruption, the eruption along the surrounding areas was explosive enough to pulverize lake sediments and country rhyolitic rocks resulting in 'fall' and 'surge' deposits known as the Rotomahana Mud.

The Taupo, Pupuke and Maungataketake basaltic samples were comparatively 'older' samples with formation dating to around 140 ka, 200–260 ka, and 35–180 ka years ago (Brown et al. 1994; Lindsay et al. 2011). Rhyolite is the predominant material (~98%) at Taupo from the past eruptions originating 300 ka ago. Although basalt is rare in Taupo, it has erupted from several vents in the region close to Lake Taupo resulting in 'red' scoria deposits of two types—'drier cones' farther from the lake and 'wetter tuff' deposits nearer to the lake (Brown et al. 1994).

Pupuke, considered to be the first volcano marking the evolution of AVF, generated ash-lapilli (gravel) rich beds (overlaying a fine tuff bed) near the crater rim of the lake. The volume of volcanic deposits was estimated to be around 0.07 km^3. Lastly, Maungataketake, a small-volume AVF volcano, showcased pheratomagmatism along with wet violent base surges. In the distal areas from the vent (as in our case), the beds were fine-grained with thin beds of angular and glassy lapilli beds (Flores et al. 2014). Eruptions like wet base surges are likely to occur in the future

in Auckland, hence their knowledge of mechanical behavior can be of significant importance.

As such in this study, the areas of tephras' collection were central and northern North Island, and included Rotorua and Taupo townships as well as Auckland city. Heterogeneous tephra samples were collected from the eruption zones, as shown in Fig. 1, and named accordingly: Kaharoa Ash (KA), Tarawera Basalt (TB), Rotomahana Mud (RM), Taupo Scoria (TS), Pupuke Basalt (PB) and Maungataketake Ash (MA). The tephras, thus, investigated included a wide array of soil types from clayey sands, and silty sands to gravelly sands as illustrated below through physical and chemical characterizations.

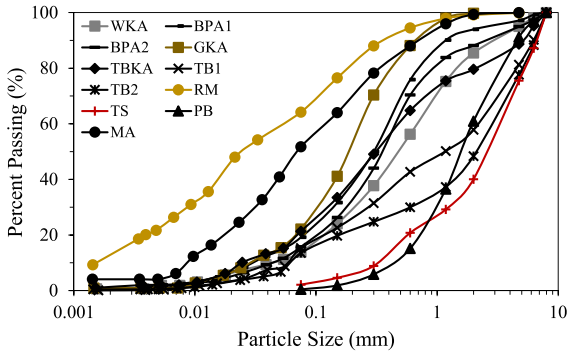

Fig. 2 Tested particle size distributions of collected tephra samples

3 Physical and Chemical Characterization

To assess the suitability as backfilling materials of the NZ tephra samples collected, firstly conventional laboratory tests were carried out, including both physical (particle size distribution, specific gravity, Scanning Electron Microscope (SEM)) and chemical (X-ray Fluorescence (XRF) and X-ray Diffraction (XRD) analyses characterizations (Rendón et al. 2020). All the materials were oven-dried at 105 °C for 24 h before carrying out the tests. The results of these are presented henceforth.

3.1 Physical Properties and Morphology (SEM)

The gradation characteristics were examined by performing sieving and hydrometer analyses (ASTM 2017a, 2017b) on three samples for each tephra type. The deposits contained particle sizes up to 50 mm. For laboratory testing purposes, only the particles passing through the 8 mm sieve were used. The particle size distribution (PSD) curves were averaged out and representative PSD curves of each tephra type are presented in Fig. 2. Based on the Unified Soil Classification System (USCS), the White Kaharoa Ash (WKA), Black Pumiceous Ashes (BPA1 and BPA2), Golden Kaharoa Ash (GKA), and Tarawera Basalt with Kaharoa Ash (TBKA) samples classified as well-graded silty sands (SW-SM). The Taupo Scoria (TS) sample is classified as well-graded gravel (GW). The Tarawera Basalts (TB1 and TB2) are categorized into poorly-graded silty sand (SM) and silty gravels (GM) respectively. The Pupuke Basalt (PB) is designated as a poorly graded sand (SP) with an almost negligible amount of fines. The Rotomahana Mud (RM) tephra is classified as a low-plasticity clayey-sand (CL) with liquid limit LL = 36.8%, plastic limit PL = 23.8%, and plastic index PI = 13.0%; along with the Maungataketake Ash (MA) as sandy silt (ML) sample with LL = 30.1%, PL = 26.4% and PI = 3.7% (ASTM 2017c). Being base surge deposits, both RM and MA samples exhibited low plasticity. Except for RM and MA samples, the remaining samples contained non-plastic fines. The index properties are as such reported in Table 1.

Based on the SEM results carried out at 150× magnification and 100 µm scaling (Fig. 3) on 0.075 mm fraction size, the texture of the tephras categorized as vesicular type containing voids within and on the surface (Gobin et al. 2023). The rhyolitic WKA and BPA samples contained fibrous, glassy, and highly angular particles enclosing elongated voids ('stretch marks' or 'layers' type of voids). The TB and TS samples, though both basaltic in origin, also differed in terms of their shape and appearance. TB pertained a subangular blocky, sponge-like structure with larger voids on a rough surface (Plinian type deposit produced after the significant rise of pulverized gas and ashes); while the TS showcased angular, sharp-edged and jagged topography with uneven distribution of voids (Strombolian type deposit generated as short bursts of lava near vent). The RM sample had a dusky-chalky (softer) appearance due to hydrothermal alteration (Lowe and Balks 2019; Heap and Violay 2021) of previous country rocks and rhyolitic rocks with very small voids on the surface.

Table 1 Index properties of tephra samples

Tephra sample	Gravel (%)	Sand (%)	Fines (%)	PI (%)	D_{50} (mm)	C_u	C_c	Soil classification
WKA	5.0	81.2	13.8	NP	0.50	16.3	1.5	Silty sand (SM)
BPA1	2.8	78.0	19.2	NP	0.30	13.7	1.6	Silty sand (SM)
BPA2	5.1	79.2	15.7	NP	0.37	11.1	1.6	Silty sand (SM)
GKA	0.3	77.6	22.1	NP	0.20	7.7	1.4	Silty sand (SM)
TBKA	11.3	67.4	21.3	NP	0.32	20.9	1.3	Silty sand (SM)
TB1	18.7	66.0	15.3	NP	1.16	38.3	0.6	Silty sand (SM)
TB2	22.3	64.1	13.5	NP	2.16	49.4	1.9	Silty sand (SM)
RM	0.1	35.7	64.2	13.0	0.03	42.3	0.7	Sandy lean clay (CL)
TS	24.5	73.4	2.1	NP	2.77	10.8	1.3	Silty sand (SM)
PB	8.9	90.7	0.4	NP	1.63	4.5	1.2	Poorly-Graded sand (SP)
MA	–	48.3	51.7	3.7	0.07	14.5	0.9	Sandy silt (ML)

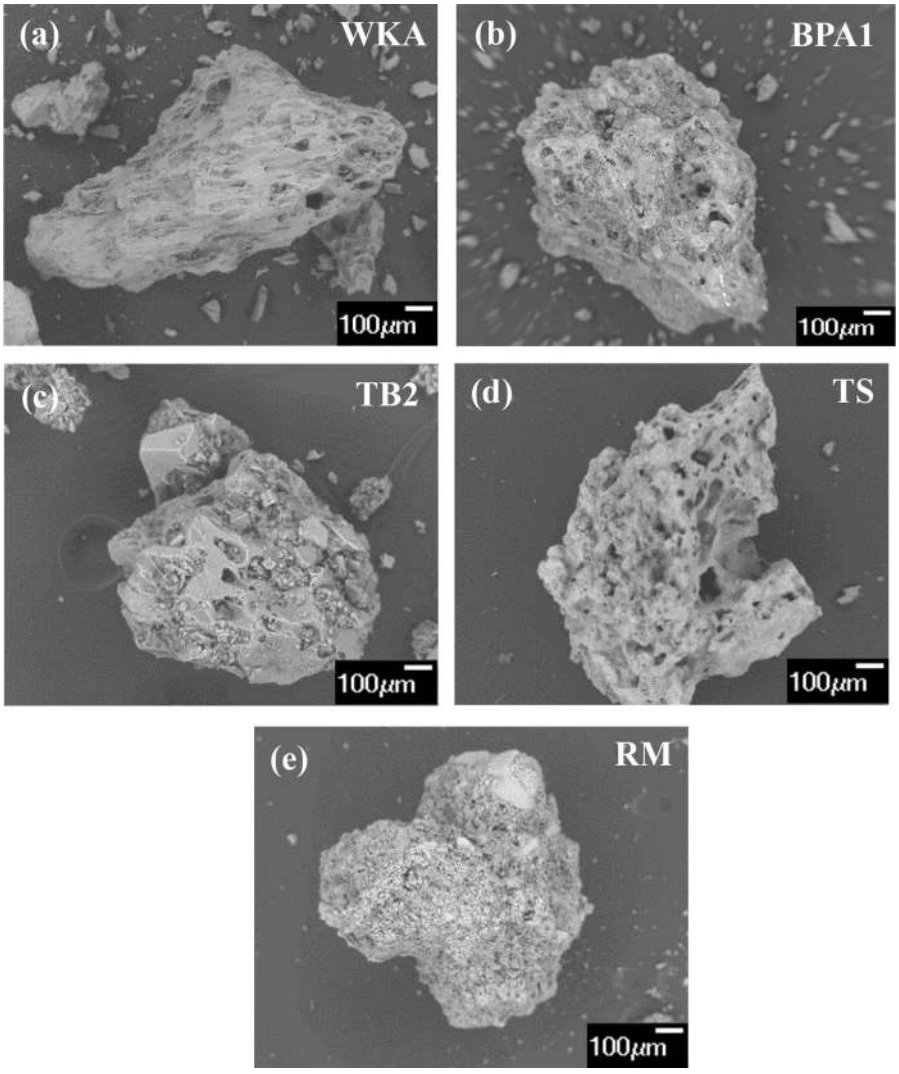

Fig. 3 Morphology (shape, structure and voids) of selected tephras

As indicated through the visual observations and SEM images, owing to the presence of internal voids and different types of tephra in the bulk sample, the specific gravity (G_s) might be different among individual particles of a particular size as well as different fraction sizes of a particular tephra. The estimation of G_s was, therefore, made for all fractions (Table 2) by water pycnometer and vacuum application (ASTM 2014). The pycnometer was continually agitated under a vacuum for at least 2 h to ensure suspension of tephra and removal of air from within.

Over the investigated range of particle sizes for the tephras, the G_s values for WKA, BPA2, PB, and TS samples showed the greatest change with the variation in particle size—i.e., the trend followed a decreasing pattern with the increase in particle size (Fig. 4), with the highest percentage decrease for WKA (25.8%), then BPA2 (22.1%), followed by PB (15.2%), TS (13.9%) and MA (3.2%). The reason behind this could be attributed to the smaller amount of internal voids into which water could not penetrate upon the decrease in particle size to around 0.075 mm (Wesley 2001; Cecconi et al. 2010; Stringer 2019).

On the other hand, the rhyolitic GKA sample showed a marginal decrement of 1.0% in G_s in comparison to the other rhyolitic WKA and BPA2 samples. The basaltic PB, TS, and MA samples showed a lower decrement in G_s values with the increase in particle size than the rhyolitic WKA and BPA2 samples. This could be further attributed to the nature of the formation of different tephras with rhyolitic being more gaseous than basaltic, therefore, leading to more internal voids. On the contrary, the G_s values of the RM sample appeared to showcase an increasing trend from 0.15 to 2.00 mm due to intermixed basaltic fractions.

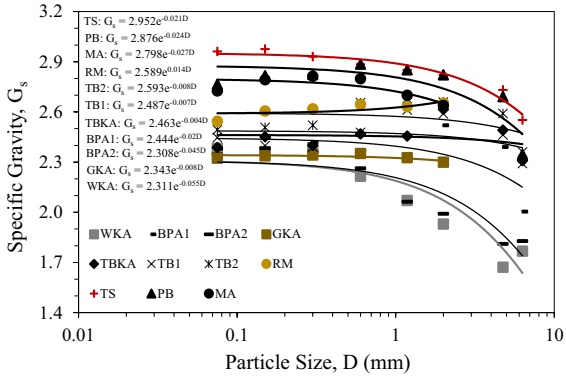

Fig. 4 Specific gravity values of investigated fractions of tephras

Some irregular trends were also observed for basaltic TB1, TB2, and intermixed BPA1, TBKA samples. For TB2, the G_s showed an increase from 6.30 mm to 0.60 mm particle size, and thereafter a decrease from 0.60 mm up to fines. There appeared to be a similar trend for TB1, though the increase in G_s was apparent up to 1.18 mm, below which the G_s seemed to decrease. Similarly, for TBKA and BPA1, the increase in G_s was apparent only from 6.30 mm to 2.00 mm particle size, below which G_s reduced considerably. Also, the G_s values of TBKA were comparatively higher than BPA1 (and similar to TB1

Table 2 G_s values of investigated fractions of all tephras

Tephra sample	Specific gravity (G_s)								
	6.30 mm	4.75 mm	2.00 mm	1.18 mm	0.60 mm	0.30 mm	0.15 mm	0.075 mm	< 0.075 mm
WKA	1.767	1.671	1.929	2.070	2.215	2.386	2.363	2.382	2.372
BPA1	2.003	2.389	2.519	2.318	2.368	2.420	2.445	2.379	2.341
BPA2	1.827	1.810	1.990	2.062	2.262	2.360	2.381	2.346	2.370
GKA			2.299	2.327	2.352	2.343	2.337	2.323	2.284
TBKA	2.309	2.491	2.616	2.455	2.469	2.399	2.452	2.387	2.433
TB1	2.291	2.462	2.588	2.612	2.477	2.390	2.398	2.446	2.393
TB2	2.360	2.590	2.658	2.679	2.655	2.520	2.507	2.493	2.456
RM			2.653	2.631	2.645	2.618	2.605	2.544	2.569
TS	2.551	2.732	2.820	2.850	2.884	2.930	2.975	2.961	2.962
PB	2.345	2.691	2.822	2.851	2.885	2.824	2.816	2.765	2.690
MA			2.638	2.700	2.798	2.813	2.793	2.726	2.701

and TB2) in the range between 6.30 and 2.00 mm, indicating definite intermixing between rhyolitic and basaltic components. Contrary to BPA2, BPA1 also seemed to include basaltic fractions in it (as evident from higher G_s values in the range 6.30–0.60 mm).

Intermixing among different types of deposits is a common occurrence due to the flow and redeposition of tephra deposits. Due to intermixing, the G_s of the bulk sample is different from the G_s of the individual fractions of a certain tephra deposit. Therefore, the G_s of the bulk sample were taken into account and calculated as:

$$G_s = \sum_{i=1}^{9} G_{si}.x_i \quad (1)$$

where G_{si} is the specific gravity value of a certain grain size and x_i is the percentage of tephra particles that have G_{si}.

To obtain the best possible estimate of G_s of tephra deposits, a comparison was made between original fines, fines produced by crushing bulk sample (below 8.00 mm), and bulk sample (Fig. 5). For WKA, BPA2, and TS samples, the bulk sample showed the lowest G_s values and nearly identical G_s values evaluated out for original and crushed bulk fines. The latter similarity indicated identical types of tephra deposits in these samples. The GKA sample, in comparison to WKA, showed lower G_s for original bulk fines due to reworked fines (below Rotomahana mud) and finer-grained composition.

For BPA1 and TBKA, the G_s values seemed to be close-ranged, indicating the dominant role played by a higher percentage rhyolitic component present in particle size < 2.00 mm suppressing higher G_s of lower percentage > 2.00 mm basaltic fractions. Likewise, the RM and MA samples also seemed to have slight differences, although the presence of slightly plastic fines played a major role in deciding closer G_s values here. Lastly, the crushed fines of bulk samples TB1, TB2, and PB presented significantly higher G_s values (11.0, 7.5, and 7.8% respectively) than original bulk fines due to the predominance of gravelly basalt in their gradation.

Overall, based on all the G_s results, the majority of the tephras could be classified as light-weight materials except for TS, PB, and MA samples which showcased G_s values higher (Aldeeky and Al Hattamleh 2018; Francisca and Bogado 2019) than 2.682 (G_s of hard-grained quartz geomaterials such as New Brighton beach sand; Sood et al. 2022a). The lower G_s values could be attributed to the abundance of lighter minerals with a range of 70–95% (Yamada 1988). Within the minerals category, the relative presence can be arranged as non-colored volcanic glass > > plagioclase feldspars > > silica minerals (quartz, cristobalite, and tridymite) ≈ mica. These minerals can have a further influence on the mechanical characteristics and therefore need quantification. The relative quantification of these minerals in respective tephras is described next in the chemical properties section.

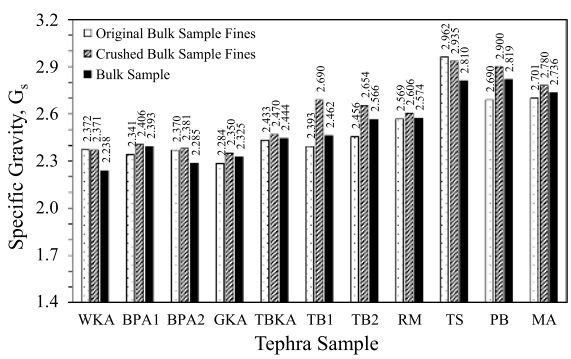

Fig. 5 A comparison of G_s of (i)—original bulk fines, (ii) bulk crushed into fines and (iii) bulk sample as a whole

3.2 Chemical Properties: Elemental State and Degree of Weathering (XRF) and Mineralogical Composition (XRD)

3.2.1 Elemental State and Degree of Weathering by X-ray Fluorescence (XRF)

To establish chemical configurations, the X-ray fluorescence (XRF) analyses were performed firstly for major oxide elemental composition (Table 3) and loss of ignition (LOI) determinations respectively. The LOI tests were carried out by heating the samples to 1000 °C. The studied tephras constituted major element oxides ranging between 45.73 and 75.10% SiO_2, 0.15–2.25% TiO_2, 11.72–17.23% Al_2O_3, 1.30–13.82% Fe_2O_3, 0.06–0.17 MnO, 0.23–13.23% MgO, 1.09–12.09% CaO, 2.26–3.90% Na_2O, 0.40–3.38% K_2O, 0.04–0.50% P_2O_5 and 0.20–8.11% LOI values indicating a wide variation from basalts to rhyolites. Also, as evident from the major element oxides of

Table 3 Major oxide analyses (XRF) of tephra samples

Tephra sample	Major oxide (Wt.%)											
	SiO_2	TiO_2	Al_2O_3	Fe_2O_3	MnO	MgO	CaO	Na_2O	K_2O	P_2O_5	LOI	Total
WKA	75.10	0.15	12.27	1.30	0.06	0.23	1.11	3.90	3.38	0.04	2.02	99.55
BPA1	72.62	0.23	12.41	2.06	0.07	0.53	1.95	3.71	2.68	0.07	3.52	99.83
BPA2	73.16	0.20	12.38	1.81	0.06	0.53	1.70	3.71	3.09	0.05	3.09	99.80
GKA	70.74	0.23	13.87	1.79	0.07	0.23	1.09	3.58	2.77	0.05	5.52	99.92
TBKAc	53.83	0.76	16.67	9.37	0.16	5.46	10.07	2.31	0.94	0.17	0.20	99.93
TBKAm	72.21	0.25	12.82	2.51	0.07	0.88	2.56	3.70	2.48	0.06	2.10	99.64
TBKAf	68.47	0.25	12.26	2.03	0.07	0.41	1.48	3.34	3.04	0.11	8.11	99.58
TB1	57.41	0.65	15.82	7.85	0.14	4.37	8.25	2.50	1.32	0.15	1.44	99.90
TB2	54.86	0.72	16.47	8.94	0.15	5.04	9.39	2.26	1.06	0.18	0.89	99.96
RM	68.19	0.40	14.87	3.91	0.08	1.22	2.58	2.29	2.80	0.09	3.61	100.04
TS	49.47	1.00	17.23	10.73	0.16	6.16	12.09	2.34	0.40	0.19	0.16	99.94
PB	45.73	2.25	11.72	13.82	0.17	13.17	8.34	2.53	0.87	0.50	0.58	99.69
MA	57.26	1.37	12.29	8.30	0.11	5.23	6.60	2.44	1.64	0.38	4.00	99.73

TBKA shown here in three size fractions to showcase intermixing, bulk wise TBKA was labelled as rhyolitic owing to major sand (i.e. TBKAm) proportion

TBKAm (1.18 mm—fines) and TBKAf (< 0.075mm) in comparison to TBKAc (6.30–2.00 mm), the TBKA sample showed signs of intermixing with Kaharoa ash as the major component (89.8%—TBKAm and TBKAf) and Tarawera basalt as the minor component (11.3%—TBKAc).

It is desired that the tephra sample to be used as land reclamation material can withstand the external atmospheric conditions for a long time and not decompose readily after a shorter period. After the release of tephra into the atmosphere, significant changes in mineral chemistry occur, which ultimately result in weathering. Depending on the nature of deposition and accompanied weathering changes (Rendón et al. 2020), elements such as Si, Al, Fe, Na, K, Ca, and Mg in tephras get depleted. To measure the amount of weathering induced, several weathering indices have been developed by different researchers using the major elemental composition (Table 4).

A particular weathering index measures the relative depletion of mobile elements to immobile elements. Mobile-to-immobile ratios are mostly used in many indices. The major oxides commonly known as alkali and alkaline oxides SiO_2, Na_2O, K_2O, CaO, and MgO are considered to be mobile (decreasing) while the remaining major oxides Al_2O_3, Fe_2O_3, and TiO_2 (known as sesquioxides) are considered to be immobile (constant). Therefore, these weathering indices have been accordingly used and described below along with their corresponding values shown in Fig. 6.

Table 4 List of weathering indices studied

Weathering index	Formula	References
Ruxton ratio (RR)	SiO_2/Al_2O_3	Ruxton (1968)
Weathering index of parker (WIP)	$100 \times [(2Na_2O/0.35) + (2K_2O/0.25) + (CaO/0.70) + (MgO/0.90)]$	Parker (1970)
Index of laterization (IOL)	$100 \times (Al_2O_3 + Fe_2O_3)/(SiO_2 + Al_2O_3 + Fe_2O_3)$	Schellmann (1981)
Chemical alteration index (CIA)	$100 \times (Al_2O_3)/(Al_2O_3 + Na_2O + K_2O + CaO)$	Nesbit and Young (1982)
Chemical weathering index (CWI)	$100 \times (TiO_2 + Al_2O_3 + Fe_2O_3)$/All chemical components	Sueoka (1988)
Chemical index of weathering (CIW)	$100 \times (Al_2O_3)/(Al_2O_3 + Na_2O + CaO)$	Harnois (1988)
Plagioclase index of alteration (PIA)	$100 \times (Al_2O_3 – K_2O)/(Al_2O_3 + CaO + Na_2O – K_2O)$	Fedo et al. (1995)

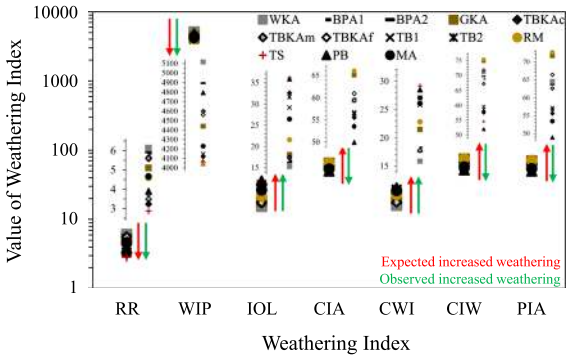

Fig. 6 Values of studied weathering indices for all tephras

The Ruxton Ratio, RR (Ruxton 1968), keeps aluminium immobile during the weathering process. The RR for a fresh sample is > 10, and this value decreases with the increase of weathering. The RR values evaluated out to be in the range 2.9–6.1 indicating higher weathering for basaltic TS (2.9) and PB (3.9), andesite basaltic TBKAc (3.2) and TB (3.3–3.6) samples; followed by intermediate weathering for dacitic RM (4.6) and basalt andesitic MA (4.7) deposits and relatively lower for rhyolitic and dacitic GKA (5.1), TBKA—m and f (~ 5.6), BPA (~ 5.9) and WKA (6.1) samples.

The Weathering Index of Parker, WIP (Parker 1970), used for silicate rocks is based on the proportions of alkali and alkaline earth metals (Na, K, Ca, and Mg) remaining after weathering. For a given rock or tephra, the optimum fresh and weathered values of WIP are > 100 and 0 respectively. The decreasing order of weathering pattern by WIP was as follows: RM ≈ TB2 ≈ TS (4040.9–4068.7) > TB1 ≈ TBKAc (4117.2–4148.7) > MA (4230.3) > GKA (4443.0) > TBKAm ≈ TBKAf (4561.8–4597.6) > BPA1 (4601.5) > PB (4796.5) > BPA2 (4893.8) > WKA (5116.7). Our WIP data were in the zonal range of those published by Fiantis et al. (2010) (~ 3800) and much higher to those published by Souri et al., (2006) (2.8–11.0). Previously, Price and Velbel (2003) reported that the WIP of felsic metamorphic rocks was 2625–15,079. The seemingly low WIP values for RM, MA, and GKA samples could be explained by their phreatomagmatic and hydrothermal alterations (Flores et al. 2014; Lowe and Balks 2019; Heap and Violay 2021), making these samples to be altered by weathering processes. Accordingly among all the samples, the WKA was the least altered and TS the most altered.

The Index of Laterization, IOL (Schellmann 1981), based on sesquioxides ($Al_2O_3 + Fe_2O_3$) to SiO_2 mass ratio showed the following decreasing order of weathering intensity: TS ≈ PB (35.8–36.1) > TBKAc ≈ TB2 (31.7–32.6) > TB1 (29.2) > MA (26.5) > RM (21.6) > GKA (18.1) > TBKAm ≈ TBKAf (17.3–17.5) > WKA ≈ BPA1 ≈ BPA2 (15.3–16.6). The trend suggested granular Taupo and Auckland basalts to be most weathered and the rhyolitic and dacitic TBKAm, TBKAf, WKA, and BPA samples to be the least weathered.

The Chemical Index of Alteration, CIA (Nesbit and Young 1982), measures the extent of conversion of feldspars to clayey minerals such as kaolinite. The CIA values for fresh tephras are ≤ 50, and these values are ≥ 100 for heavily weathered tephras (Fontoura et al. 2023). The CIA values ranged from 50.0 to 66.0 for the tephras, indicating that the samples were slightly weathered. In the A–CN–K diagram and SiO_2–Al_2O_3–Fe_2O_3 plot (Fig. 7), the samples were located in the slightly weathered region and near the SiO_2 portion respectively, suggesting that the samples were fresh or very less weathered and nearing kaolinization indicating the beginning stages of weathering.

The CIA using K_2O was modified by excluding K_2O resulting in an index known as the Chemical Index of Weathering, CIW (Harnois 1988). The optimum value of CIW varies as ≤ 50 and increases up to 100 as the weathering intensity increases. The CIW values of the studied tephras ranged from 51.9 to 75.3, indicating slight weathering and lesser clay minerals. Likewise, the Plagioclase Alteration Index PIA (Fedo et al. 1995) developed as an alteration to the CIW attains values of 50 in non-weathered tephras and 100 for clayey minerals such as kaolinite, illite, and gibbsite containing tephras (similar to ones obtained by CIA formula). The values obtained ranged from 50.0 to 71.3 indicating slight weathering.

Lastly, the Chemical Weathering Index, CWI (Sueoka 1988), is based on the increasing tendency of sesquioxides with weathering. Based on the CWI values obtained ranging between 15.8 and 22.8%, the rhyolitic samples such as WKA seemed to be least weathered or fresh followed by minor or slight alterations in BPA, TBKAm, and moderate ones in GKA and dacitic TBKAf and RM samples. The basalt andesitic TBKAc, TB, MA, and basaltic TS and PB

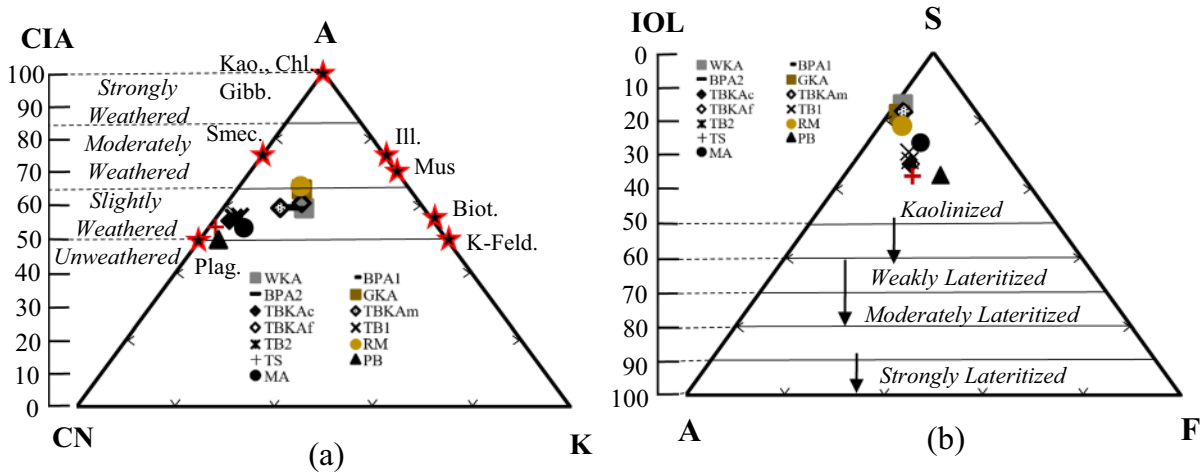

Fig. 7 **a** A–CN–K and (A—Al_2O_3; C—CaO; N—NaO; K—K_2O; Plag.—Plagioclase; K-Feld—Potassium Feldspar; Biot.—Biotite; Mus.—Muscovite; Ill—Illite; Smec. Smectite; Kao.—Kaolin; Chl.—Chlorite and Gibb.—Gibbsite), **b** S–A–F (S—SiO_2; A—Al_2O_3 and F—Fe_2O_3) ternary plots

positioned on the higher end of the weathering state based on their CWI values due to higher inclusion of sesquioxides (Al_2O_3, Fe_2O_3, and TiO_2) as a result of their weathering processes.

Out of the studied weathering indices, the IOL and CWI tended to show an increasing trend with the increase in weathering intensity whereas the RR, WIP, CIA, CIW, and PIA showcased a decrement with the increase in weathering. Further on, the trends for weathering indices namely WIP, RR, IOL, and CWI agreed with their expected trends of weathering whereas those for CIA, CIW, and PIA showed the opposite behaviour.

Using the above information, the relationship between chemical indices and weathering state was established, as shown in Fig. 8. Based on the international classification for weathering (Hatheway 2009), the tephras could be classified as fresh or slightly weathered (Table 5). Three types of correlations: low ($R^2 = 0.34$ for WIP), moderate ($R^2 = 0.49$–0.70 for CIA, PIA, CIW), and high ($R^2 = 0.83$–0.89 for IOL and CWI) seemed to exist. Though the trend for RR seemed to be an expectedly negatively correlated state (moderate correlation of $R^2 = 0.70$) with the weathering state, RR has to be considered appropriately further due to the involvement of only two components (SiO_2 and Al_2O_3).

The WIP, CIA, CIW, and PIA are based on the groups of mobile oxides. The decreasing trends and corresponding values of CIA, CIW, and PIA from silty sandy Rotorua rhyolites to gravelly sandy Auckland basalts suggested that feldspars conversion (primary minerals) to clays (secondary minerals) was lesser. Because CIW and PIA do not consider aluminum associated with K-feldspar, they yielded higher values for K-feldspar-rich tephras, irrespective of their chemical weathering or not (Fedo et al. 1995). This is evident from the correlation values of CIW ($R^2 = 0.68$), PIA ($R^2 = 0.56$), and CIA ($R^2 = 0.49$).

The WIP showed the lowest correlation ($R^2 = 0.34$) with the weathering state in comparison to the other weathering indices (Fig. 8b). The WIP is the only index to consider aluminum as mobile in comparison to the remaining indices and is purely based on the alkali and alkaline earth elements. This characteristic was used to study and get the best fit through chemically heterogeneous tephras in this study (Price and Velbel 2003). Based on the principle of WIP, as the values get smaller, the samples are more weathered and older. Also, with more weathering, the SiO_2 is expected to be lost along with mobile Na_2O, K_2O, CaO, and MgO, thus decreasing WIP (and increasing CWI). Also, the trends for CWI and IOL increased with weathering due to the depletion of Si and increment of Fe and Ti (Fig. 8c).

Therefore, in order to properly characterize different tephra deposits, the following conditions were considered: parent rocks (homogeneous or

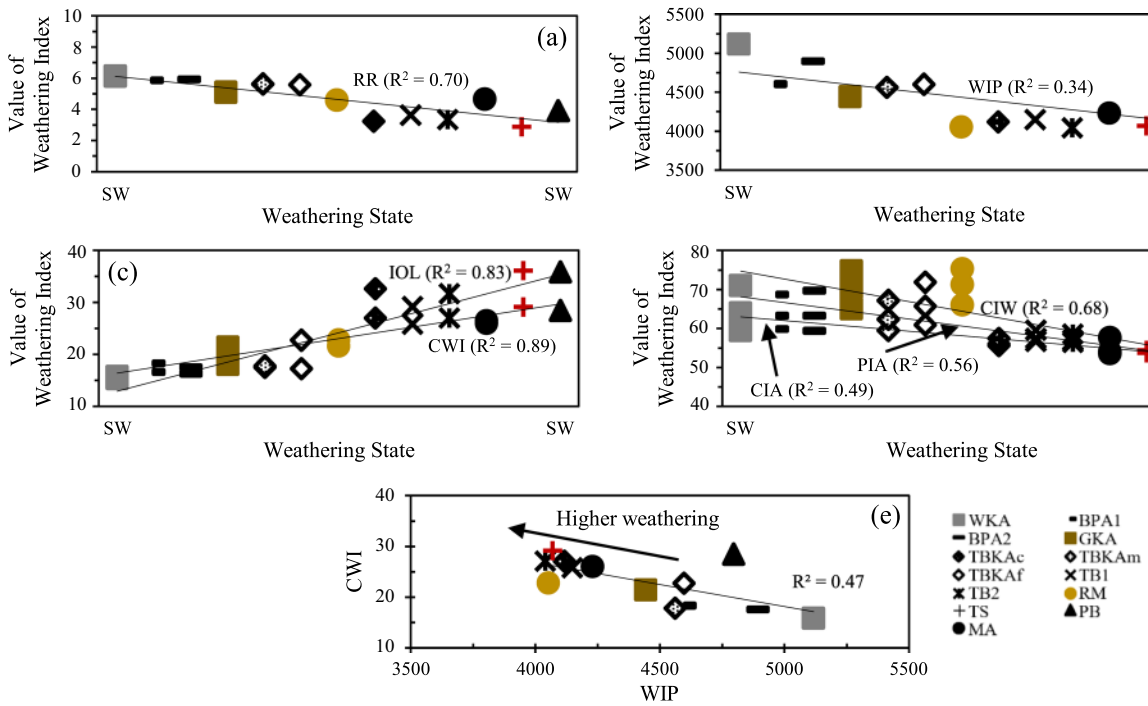

Fig. 8 Relationships between weathering state and used weathering indices (**a**–**d**) and suited weathering indices (WIP vs. CWI) for the investigated tephras (**e**)

Table 5 Classification of rock weathering

Grade	Classifier	Typical characteristics
I	Unweathered (UW) or fresh (F)	Unchanged from original state
II	Slightly weathered (SW)	Slight change in colour or slight weakening, otherwise similar to UW or F
III	Moderately weathered (MW)	Material is weakened, penetrative change in colour, large pieces cannot be broken by hand
IV	Highly weathered (HW)	Large pieces can be broken by hand, does not disintegrate (slake) when dry sample is immersed in water
V	Completely weathered (CW)	Considerably weakened, slakes, original texture visible
VI	Residual soil (RS)	Soil derived by in situ weathering but no original texture or fabric retained

heterogeneous), aluminum mobility, and many mobile oxides. The selection of weathering indices such as CIA, CIW, and PIA were avoided due to opposite weathering trends observed. Also, weathering indices RR, VRI, and IOL were not selected despite possessing higher correlations against the weathering state due to lesser mobile elemental oxides in their formulation. Considering the stated, the weathering indices WIP and CWI were selected for further assessment of engineering properties. The correlation between them is shown in Fig. 8e.

3.2.2 Mineralogical Composition by X-ray Diffraction (XRD)

In supplement to the major oxides, the array of minerals was established through the X-Ray Diffraction (XRD)—Rietveld analysis. Using the same, the relative amounts of crystalline phases and amorphous contents in the tephras are presented in Table 6.

An illustrative example showing the amorphous phase and other crystalline phases is presented for rhyolitic WKA in Fig. 9. The presence of amorphous

Table 6 Modal composition results of XRD-Rietveld analyses for studied tephras

Mineral (Wt. %)	Tephra												
	WKA	BPA1	BPA2	GKA	TBKAc	TBKAm	TBKAf	RM	TB1	TB2	TS	PB	**MA**
Glass	78.3/0	81.8/0	57.9/0	86.2/0	59.4/0	67.3/0	79.6/0	13.9/0	26.9/0	21.2/0		31.5/0	38.4/0
Quartz (Q)	3.7/17.2	5.3/29.0	10.5/24.8	3.3/24.1	1.0/2.4	7.1/21.6	5.1/25.0	26.2/30.5	5.3/7.2	3.0/3.8	1.7	1.3/2.0	26.6/43.1
Cristobalite (C)	0.6/2.7	1.6/8.7	1.8/4.3	0.7/5.4	2.2/5.5	0.4/1.2	0.2/0.9	2.1/2.5	2.8/3.8	0.3/0.4	5.6		1.1/1.8
Q+C	4.3/19.9	6.9/37.7	12.3/29.1	4.0/29.5	3.2/7.9	7.5/22.8	5.3/25.9	28.36/33.0	8.0/11.0	3.4/4.2	7.3	1.3/2.0	27.7/44.9
Biotite	0.2/1.0	0.7/3.7	0.9/2.1	0.5/3.5		0.3/0.8							
Muscovite								9.6/11.2					
Albite	3.4/15.5	8.1/44.5	1.7/3.9			9.7/29.7	0.2/1.2	6.2/7.2			18.1	8.1/11.9	7.7/12.4
Oligoclase	10.1/46.8		22.5/53.3	8.1/58.4	23.5/57.8	9.2/28.1	13.5/66.2	24.8/28.8	40./54.8	52.3/66.4			
Labradorite					0.8/1.9				1.6/2.1	1.2/1.5			
Bytownite												19.5/28.4	11.7/19.0
Anorthite											37.6		
Sanidine	2.9/13.3	1.4/7.9	4.6/11.0	1.2/8.5		5.1/15.5	1.3/6.6	12.3/14.3					
Orthoclase					3.3/8.1				7.8/10.7	5.5/7.0	4.2	3.7/5.5	5.4/8.8
Augite	0.7/3.4	1.1/6.3	0.2/0.5	0.01/0.1	9.9/24.3	1.0/3.2		3.5/4.1	15.7/21.4	16.4/20.8	21.5	16.3/23.8	6.3/10.3
Forsterite												19.5/28.5	2.9./4.6
Hematite											11.4		
Total Crystal Content	21.7/100	18.2/100	42.1/100	13.8/100	40.6/100	32.7/100	20.4/100	86.1/100	73.1/100	78.8/100	100	68.5/100	61.5/100
Crystal/Glass	0.3	0.2	0.7	0.2	0.7	0.5	0.3	6.2	2.7	3.7		2.2	1.6
Alkali Feldspars (A)	2.9/13.3	1.4/7.9	4.6/11.0	1.2/8.5	3.3/8.1	5.1/15.5	1.3/6.6	12.3/14.5	7.8/10.7	5.5/7.0	4.2	3.7/5.5	5.4/8.8
Plagioclase Feldspars (P)	13.5/62.3	8.09/44.5	24.1/57.3	8.1/58.4	24.3/59.7	18.89/57.7	13.8/67.5	31.0/36.5	41.6/56.9	53.5/67.9	55.3	27.6/40.3	19.3/31.4
Feldspars (F)	16.4/75.6	9.5/52.4	28.7/68.3	9.3/66.9	27.6/67.8	23.95/73.2	15.1/74.1	43.3/51.0	49.4/67.6	59.0/74.9	59.5	31.3/45.8	24.7/40.2
Accessories (Acc.)*	1.0/4.4	1.8/10.0	1.1/2.6	0.5/3.5	9.9/24.3	1.3/4.0		13.2/15.5	15.7/21.4	16.4/20.8	33.2	35.8/52.3	9.2/14.9
R_{wp}	6.0	9.4	9.2	9.7	13.1	21.9	8.2	13.1	12.3	12.4	14.0	10.7	13.3
GOF	1.1	2.7	2.7	2.2	3.2	9.2	1.6	5.7	5.4	5.5	7.0	4.3	4.6

Plagioclase feldspars: Albite, Oligoclase, Labradorite, Bytownite, Anorthite; Alkali Feldspars: Sanidine, Orthoclase

Accessories taken as the sum of the following minerals: Biotite, Muscovite, Augite, Forsterite and Hematite

Crystalline abundances normalized so that they sum to 100%

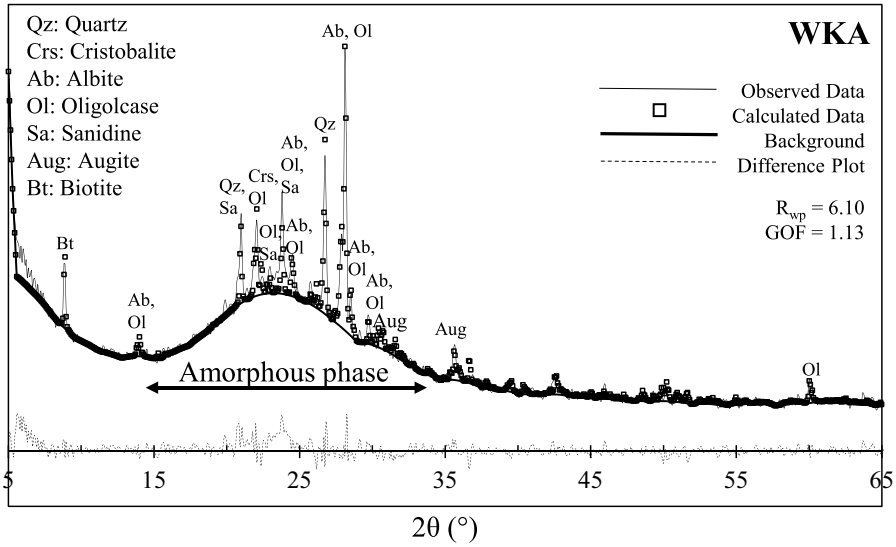

Fig. 9 Illustration of amorphous and detected crystalline phases in the XRD pattern of rhyolitic White Kaharoa Ash (WKA)

content is evident as a background hump in the XRD pattern of WKA tephra. This was also supported by high glass content ranging between 57.9 and 86.2% in rhyolitic and dacitic samples (WKA, BPA1, BPA2, GKA TBKAm, and TBKAf) as obtained from Rietveld refinement (Table 6). The basalt–andesitic TB (TB1 and TB2) and basaltic PB and MA samples constituted intermediate amounts of glass content ranging between 21.2 and 38.4%, whereas the dacitic RM contained comparatively lesser glass content of 13.9%. No amorphous content was detected in the TS sample. As also evident, the glass content of rhyolites and dacites was comparatively higher than the andesites and basalts.

In addition, the differences among the various tephra types could also be accounted for by the relative abundances of minerals. For rhyolitic and dacitic Rotorua tephras WKA, GKA, BPA, GKA, TBKAm, and TBKAf; silica minerals such as quartz and cristobalite, alkali and plagioclase feldspars were the primary minerals whereas biotite (mica) and augite (pyroxene) were present as accessories (Leonard et al. 2002; Ewart and Cole 1967). In comparison, for basalt–andesitic Rotorua samples TBKAc, TB1, and TB2 and basaltic Taupo and Auckland (TS and PB) samples, plagioclase feldspars, pyroxenes and olivines (forsterite for PB soil) were the essential minerals and secondary minerals such as hematite in TS (thus explaining its red colour) were also seen (Hiess et al. 2007; Searle 1961; Brown et al. 1994). Lastly, the dacitic RM and basalt–andesitic MA constituted a higher proportion of silica minerals indicating influences of other weathering mechanisms as discussed further. The overall susceptibility of the minerals is identified as olivine > pyroxene > mica (biotite) > plagioclase feldspar (Ca to Na) > alkali (K) feldspar > quartz (Bowen 1928). This series indicates olivine to be the most and quartz to be the least susceptible to weathering. In other words, tephra containing a lower amount of olivine or a higher amount of quartz shows relatively lower weathering potential (Goldich 1938). This is reflected in the mineralogical compositions (Table 6), wherein rhyolitic and dacitic tephras such as WKA, BPA1, BPA2, GKA, TBKAm, and TBKAf were relatively less weathered than basalt andesitic tephras such as TBKAc, TB1 and TB2 and basaltic TS and PB.

As noted above, the alkali feldspar is the last feldspar to weather before quartz. Orthoclase was present in lesser amounts in basalt andesites and basalts in comparison to plagioclases, indicating that the plagioclases suffered chemical weathering primarily in these tephras. Sanidine was the alkali feldspar of rhyolites and dacites studied. The Rotorua rhyolites and dacites were placed closer to albite (Ab) and in the intermediate region of albite (Ab)–orthoclase (Or) space, whereas the Rotorua basaltic andesites, Taupo, and Auckland basalts were positioned in the proximity of anorthite (An) region in the albite (Ab)–anorthite (An) plane (Fig. 10a). To get a better viewpoint of their compositional analyses, all the tephras were plotted in the Q–A–P (Quartz–Alkalis–Plagioclase)

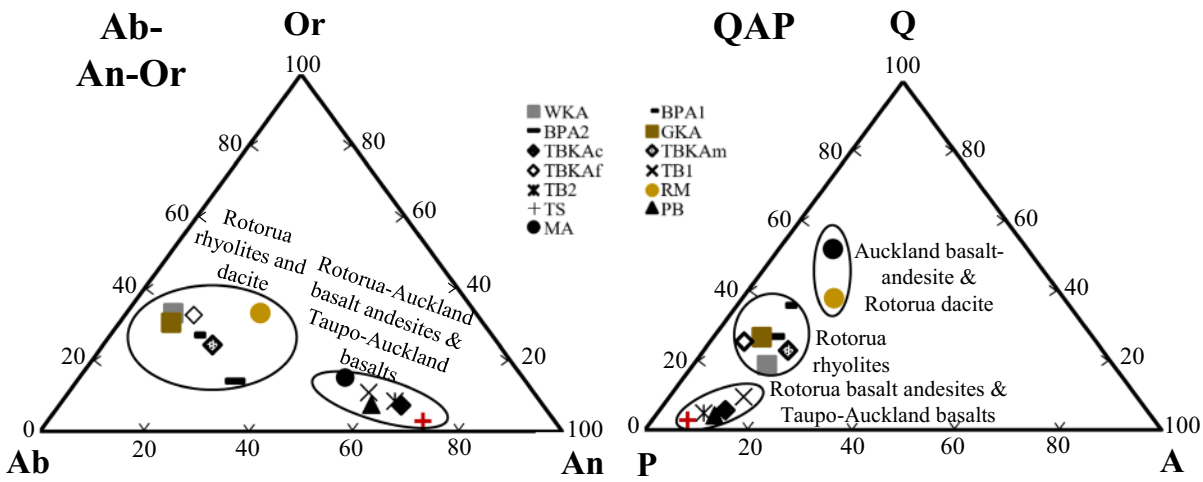

Fig. 10 Chemical analyses of the studied tephras **a** classification in Ab–An–Or space (from XRF data) and **b** weathering state in QAP space (from XRD data)

plane (Fig. 10b). All of them plotted parallel to the Q–P plane, indicating a lack of alkali feldspars in their composition.

Moreover, the analysis of the weathering state based on quartz and feldspar contents for granitic rocks was used to explain the differences in weathering conditions of studied tephras (Nesbitt et al. 1997; Torabi-Kaveh et al. 2023). The Rotorua basalt andesites TBKA (m and f), TB (1 and 2), basaltic Taupo TS, and Auckland PB plotted very close to the Plagioclase (P) section indicating slight chemical weathering in terms of mechanical breakdown, and the samples composed of bedrocks (feldspars) rather than clay minerals or quartz (Menendez et al. 2022) Slightly above them along the same Q–P plane lay the Rotorua rhyolites and dacites series which was relatively less coarser, and more quartz and alkali feldspar enriched.

On the other hand, the dacitic Rotorua RM sample belonging to a similar eruption source (i.e. OVC) as Rotorua rhyolites contained comparatively higher quartz. The RM consisted of abundant crushed sands and silt fractions (quartz and plagioclase abundant) and secondary aluminous clay minerals such as muscovite. Likewise, the basalt andesitic MA from Auckland plotted closest to the Q region in the Q–A–P plane, showing significant enrichment of quartz in proportion to feldspars. The phreatic and phreatomagmatic nature of RM (Lowe and Balks 2019) explained the mechanical disintegration of rhyolitic ash and country lithics (quartz and feldspar enrichment) and the mixing of clay and silt lake sediments (clay enrichment). Being a surge deposit like RM, the MA tephra constituted an amalgamation of basaltic lapilli with country rock lithics ultimately leading to quartz and plagioclase abundance (Flores et al. 2014). The higher locations of RM and MA in A–CN–K and Q–A–P plots, thus, indicated that external influences such as mechanical breakdown and intermixing were dominant factors and the mineralogy was not entirely controlled through chemical breakdown yet.

The studied tephras, therefore, did not appear to be achieving steady-state weathering conditions yet and were relatively fresh or slightly weathered in nature making them ideal geomaterials for further geotechnical characterization. The weathering indices and relative percentages of silica (such as quartz and cristobalite) and feldspar minerals were further used to study the effect of chemical composition on the degree of particle breakage resulting from compaction tests, as discussed in Sect. 4.

4 Compaction Characteristics and Particle Breakage Evaluation

To facilitate the use of tephras as backfilling materials, it is important to ensure sufficient densification of the constituent particles. Further investigation involving density check was carried out on six

tephra samples using the standard Proctor compaction method (ASTM 2012). The samples included Rotorua rhyolitic and dacitic (WKA, GKA, TBKA, RM) and Auckland basalt andesitic and basaltic (MA and PB) tephras. Figure 11 shows the dry density (ρ_d) and void ratio (e) versus water content (w) relationships; essentially, the maximum dry density (ρ_{dmax}) and optimum water content ($w_{opt.}$) varied from 1.32 to 1.71 g/cm^3 and 10.6 to 24.9% (lower range water content, Liu et al. 2022) for the investigated tephras. These values are also presented in Table 7.

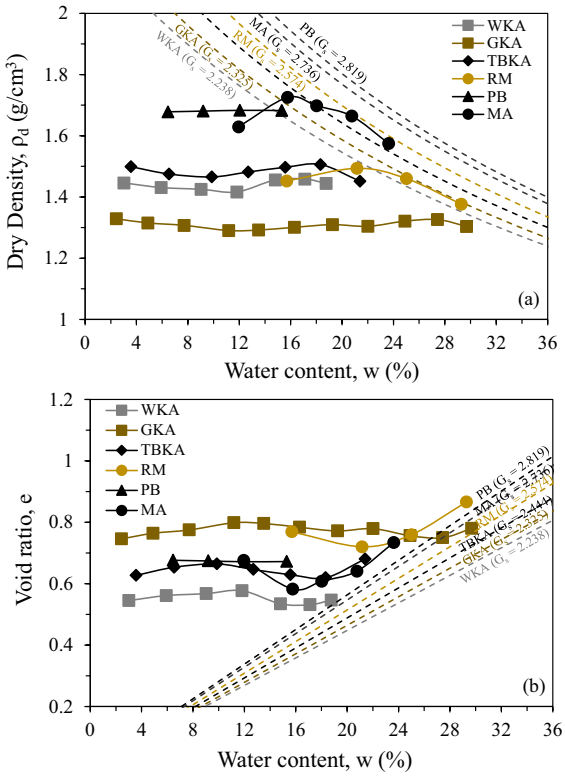

Fig. 11 Compaction curves obtained for different tephras: **a** Variations in dry density with water content; and **b** variations in void ratio with water content

Three types of compaction curves were obtained (Fig. 11): one-and-a-half peak (for WKA, GKA, and TBKA), parabolic (for RM and MA), and gentle peak (PB). The Rotorua rhyolites WKA, GKA, and TBKA being well-graded and non-plastic silty sands (14–22% fines), as also manifested by their uniformity coefficient (C_u) and curvature coefficient (C_c) values in Table 1, were more compactable owing to a wide range of particle sizes enabling better interlocking. From about $w = 2.5$–3.5%, their ρ_d decreased with the increase in w and reached a minimum at about $w = 9.0$–12.0%. With the further increase in w, ρ_d increased for values of w up to approximately 16–17% (WKA and TBKA) and 24.5–27.5% (GKA). Beyond this w, the ρ_d decreased for WKA, TBKA, and GKA. The ρ_d (at starting w) was nearly identical to ρ_{dmax} (at $w_{opt.}$), hence the curves are defined as one-and-a-half peaks that are typical of sand-dominant tephras, containing quartz and feldspars (Lee and Suedkamp 1972).

For Auckland MA and Rotorua RM samples containing 50–70% slightly plastic fines (PI = 3.7 and 13.0%), the compaction curves were more regular or parabolic in shape. The ρ_d increased, reached a peak, and, thereafter, decreased with increasing w. This behavior was attributable to the water lubrication theory for fine-grained soils.

The saturation values ranged from 72 to 85%. for silty-sands (WKA, TBKA, and GKA) and silty tephras (RM and MA) of Rotorua and Auckland. In contrast, the inclusion of water was ineffective in controlling the density of poorly graded sand PB. This

Table 7 Compaction parameters of studied tephras

Tephra sample	ρ_{dmax} (g/cm^3)	$w_{opt.}$ (%)	Void ratio (e) at ρ_{dmax}	G_s, bulk sample	Average particle breakage (%)	
					Hardin	Miura and Yagi
WKA	1.46	16.0	0.533	2.238	1.3	0.8
GKA	1.32	24.9	0.757	2.325	6.3	5.6
TBKA	1.50	16.9	0.862	2.444	1.6	2.2
RM	1.48	23.1	0.740	2.574	7.5	2.6
PB	1.68	10.6	0.673	2.819	0.1	0.3
MA	1.71	16.9	0.595	2.736	7.6	2.4

was apparent by the very small increase in ρ_d with the increase in w (Fig. 11a) and a moderate saturation value of 50%. Expectedly, the rhyolitic (WKA, GKA, TBKA) and dacitic (RM) silty sands from Rotorua were placed below Auckland basalt–andesitic silt (MA) and basaltic sand (PB) due to their lower G_s values. The differences between tephras from different geological origins and physio–chemical states are thus evident.

As the tephras are void-filled slightly-weathered materials, they are susceptible to breakage after impact loading such as compaction. After compaction, the tested tephras were oven-dried and, then, sieved to quantify the particle breakage. The breakage indices defined by Hardin (1985) and Miura and Yagi (1997) were used to cover the entire range of particle sizes as well as the generation of fines after compaction respectively.

Figure 12 presents the PSD curves following the compaction tests. For the tested tephras, the differences in positions of the grain size distribution curves (before and after compaction) were very small. This meant that the amounts of particle crushing following the compaction process were very similar. The average of the particle breakages at different water contents was, therefore, used. As also reported in Table 7,

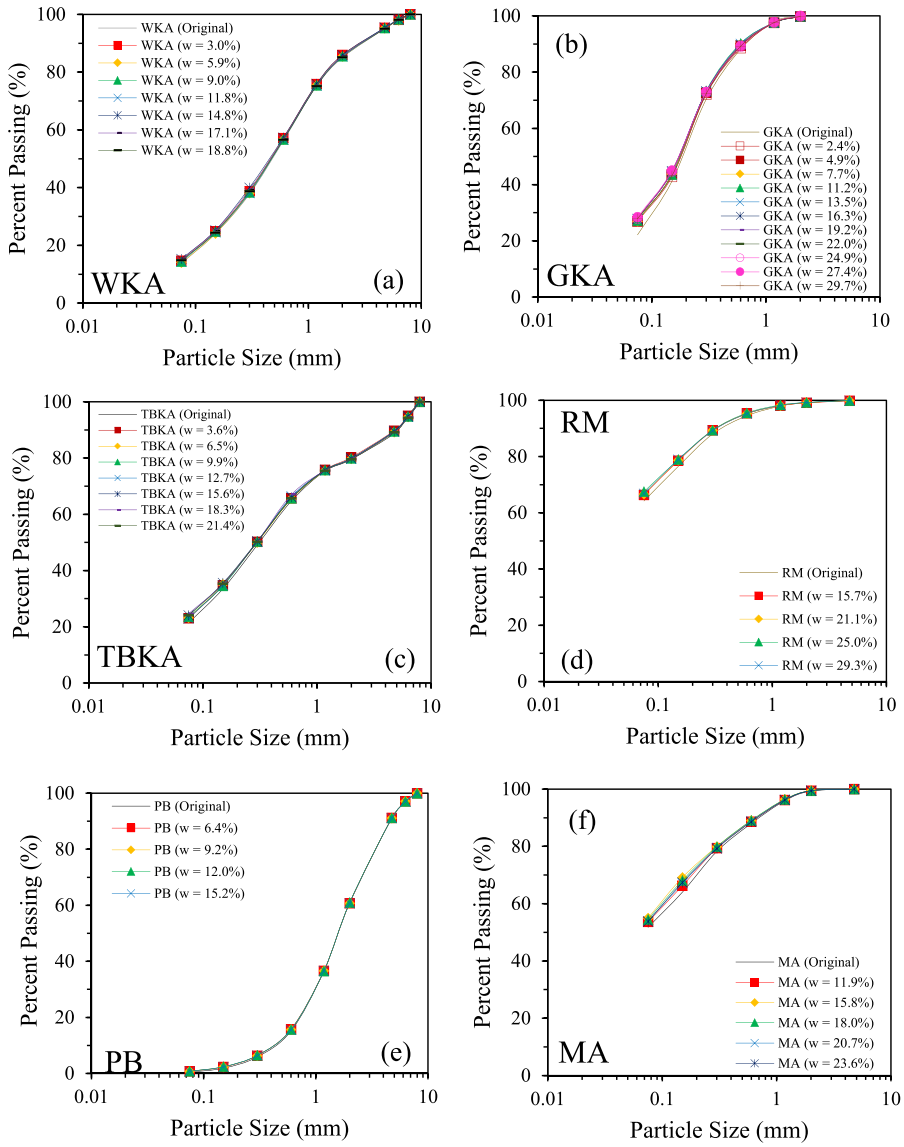

Fig. 12 Shifts in the particle size distributions after compaction at tested water contents for the tested tephras

the highest post-compaction breakage by Hardin's index was shown by fine-grained MA and RM, then friable GKA; followed by well-grained TBKA and WKA, and lastly poorly-graded PB. A slight change in breakage pattern was shown through average breakage values by Miura and Yagi's index with the friable GKA more crushable than fine-grained MA and RM; followed by well-graded WKA and TBKA and then poorly-graded PB.

Higher breakage in fine-grained soils such as RM and MA could be explained by sliding and rotation between a larger number of particles and the contact forces being weaker leading to breakage at the contact points upon compaction. In addition, the nature of deposition of these tephras (base surge deposits) was also accountable for the higher breakage. In comparison, the well-graded WKA, TBKA, and GKA showcased lesser breakage owing to better contact forces among a wider range of particle sizes. However, although being well-graded, higher breakage in GKA was due to associated weathering effects leading to pulverization and softer particles (as elaborated earlier in Sect. 3.2). For uniformly graded PB, the interlocking forces between the uniformly sized particles were negligible and additional water played very little role in bringing them together leading to insufficient compaction.

Figure 13 shows the relationship between ρ_d and breakages of different tephras. From this figure, it could be understood that the breakage in general shows an increase with the increase in ρ_d with correspondingly higher values around $w_{opt.}$ condition than at the drier or wetter conditions. This fact implied that the transmission of compaction effort was most utilized and effective in optimum conditions. The $w_{opt.}$ and ρ_{dmax} obtained can, thus, be further utilized as density parameters for their usage as backfilling materials.

5 Inter-Relating Physical, Chemical, Compaction, and Other Geotechnical Characteristics

This section describes the inter-relationships developed between the physical, chemical, and compaction aspects of the airfall tephra deposits. As seen, an evaluation of the physical and chemical properties enabled the assessment of the weathering state of the tephras, which further impacted compaction characteristics and can also possibly influence shear strength behaviour. The natural existence and weathering processes dictated a broader range of particle types from gravels to clays to be present in the tephra samples. The tephras also, therefore, had different maximum densities and optimum moisture contents according to the G_s of the particles, PSD, and grain shape of particles. The majority of them had subangular to angular grain shapes, as indicated through morphology (Fig. 3), thereby aiding compaction.

Figure 14 shows the relationship between median particle size (D_{50}) with the ρ_{dmax} and $w_{opt.}$ for the studied tephras. The ρ_{dmax} increased with increasing D_{50}. Correspondingly, the $w_{opt.}$ showed a decrease with increasing D_{50}. The differences in achievable ρ_{dmax} can be attributed to their respective G_s values. The ρ_{dmax} of Auckland samples (PB and MA) was higher than Rotorua samples (WKA, GKA, TBKA, and RM) due to higher G_s associated with the former. Concerning $w_{opt.}$, the water content required to achieve optimum conditions was expectedly higher for fine-grained (> 50% fines) RM and MA tephras followed by silty sandy WKA, GKA, and TBKA and then sandy PB with almost zero fines.

The D_{50} (= 1.63 mm) of Auckland sandy PB was substantially higher than the remaining tephras possessing D_{50} in the range of 0–0.50 mm. The coarser uniform structure of PB, therefore, subsequently required lesser $w_{opt.}$. Taking $G_s = 2.682$ of New Brighton Sand (NBS, hard-grained beach sand, Sood et al. 2022a) as the dividing line, the rhyolitic samples WKA, GKA, TBKA, and dacitic RM fell on the lighter side, and basalt andesitic MA and basaltic PB leaned towards the heavier side. Being from the same eruption source, the difference between Rotorua samples was due to the inclusion of clayey minerals such as muscovite in RM in comparison to non-plastic WKA, GKA, and TBKA. Though MA also included slightly plastic fines in higher proportion, the lower plasticity, and higher G_s did not permit lower ρ_{dmax}. Instead, higher amounts of heavier accessory minerals (augite) shifted Auckland samples PB and MA to the heavier side.

As compaction results in particle breakage, suited weathering indices WIP and CWI and mineralogical composition in terms of silica and feldspar minerals after respective weathering processes were compared against breakage values. The average breakage values were plotted in terms of all particle sizes

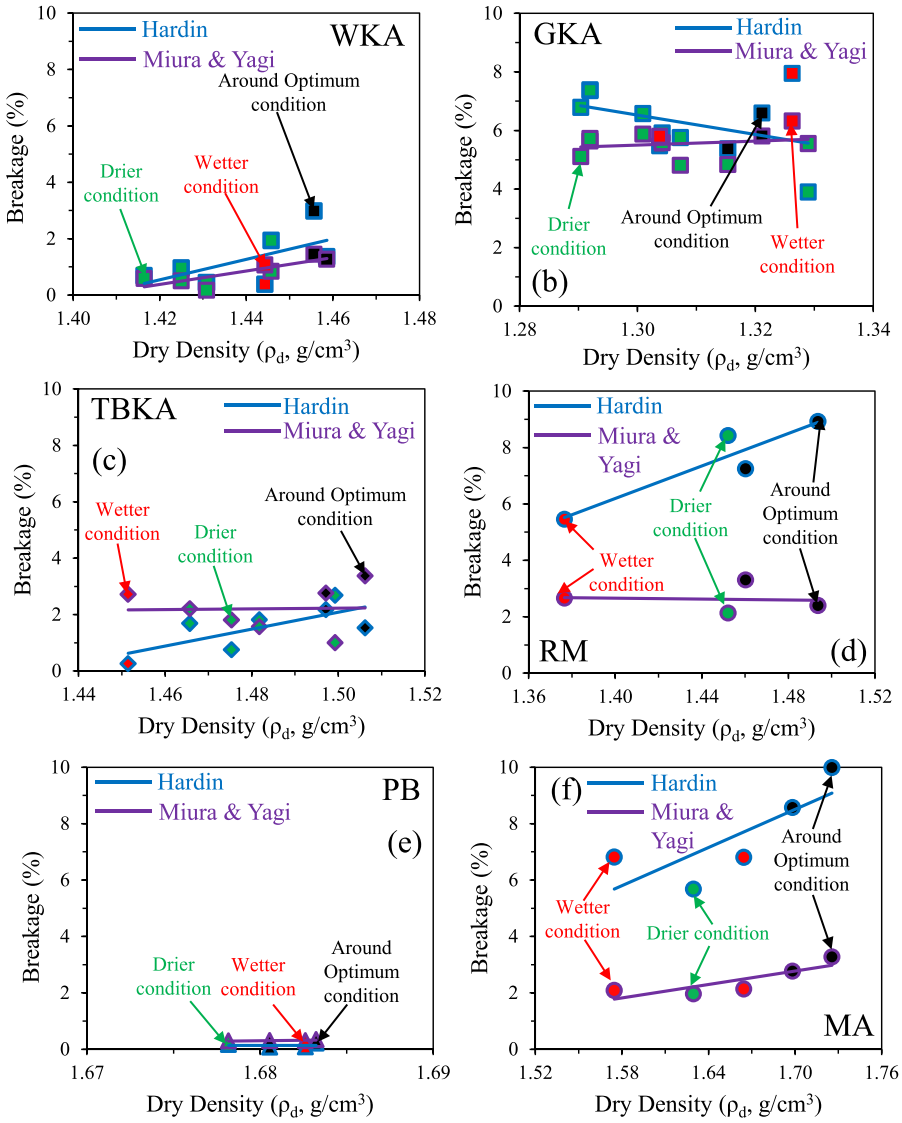

Fig. 13 Relations of overall particle size distribution (Hardin's breakage index) and increment in fines content (Miura and Yagi breakage index) and dry density after compaction

(Hardin 1985) and fine sizes (Miura and Yagi 1997). The weathering state and average breakage values for TBKA were computed by summing the respective values at its three fraction particle sizes (TBKAc, TBKAm, and TBKAf).

As established through XRD-Rietveld analyses, the amount of crystalline silica minerals such as quartz and cristobalite were highest in RM and MA; followed by GKA, TBKA, WKA, and least in PB. Considering feldspars, the Auckland samples contained lower feldspars than the Rotorua samples. As silica mineral is the last mineral to crystallize in any tephra, its resistance to weathering is highest in comparison to feldspars. However, due to external factors such as deposition and later intermixing, the balancing of silica and feldspar minerals might get affected in the host tephra. Therefore, the silica and feldspars present in the current weathered state of tephra were cumulative effects of (i) deposition manner, (ii) chemical breakdown of inherent minerals, and (iii) external intermixing if any.

As indicated by the cumulative plots of WIP and CWI (Fig. 15) against quartz–feldspar balancing (lower WIP and higher CWI values indicated higher weathering), the RM and MA samples showed higher quartz (PB being an exception showing very low silica content) and correspondingly lower feldspars than WKA, TBKA and GKA. The GKA was silica

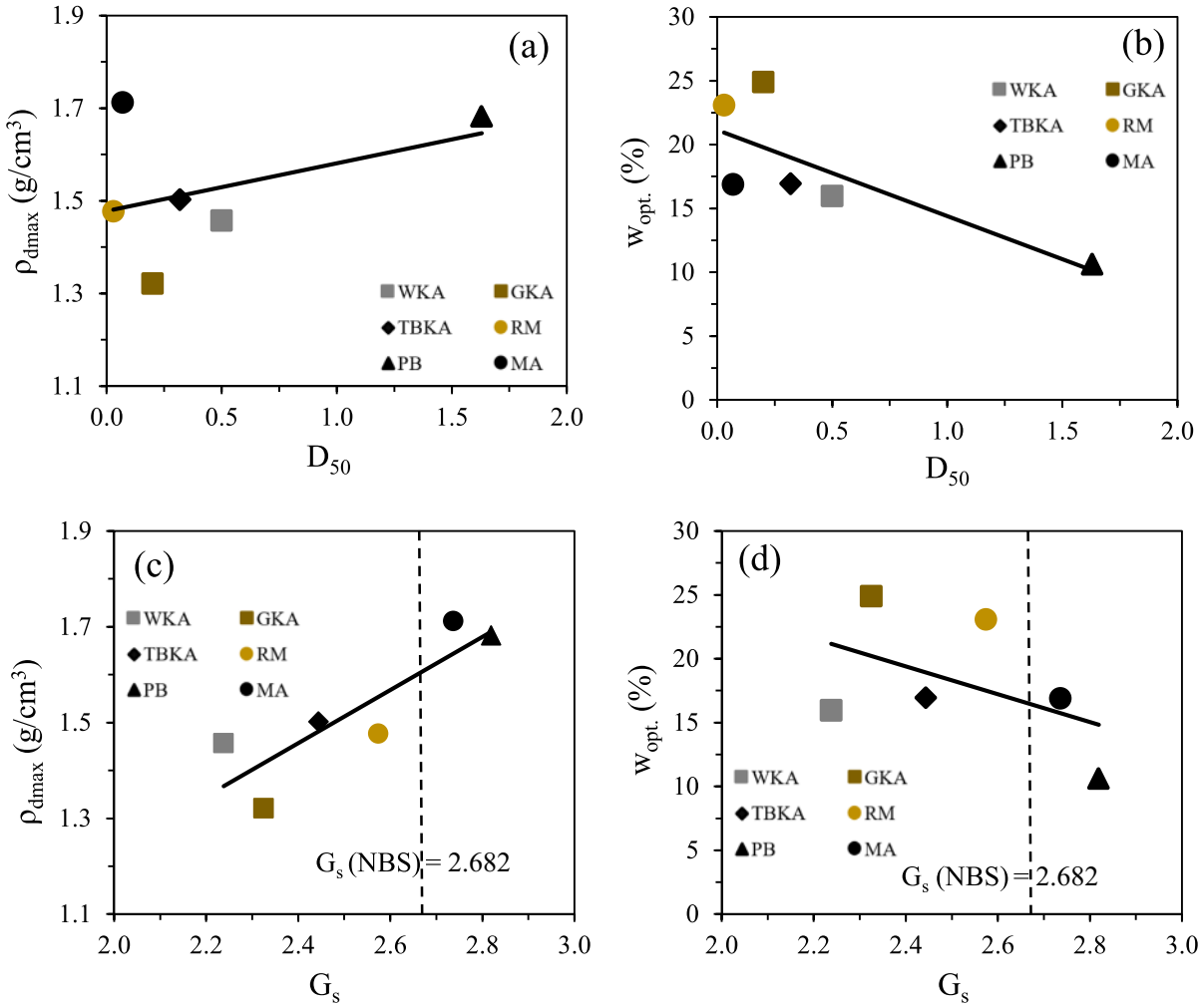

Fig. 14 Variation of median particle size D_{50} (mm) and specific gravity G_s with maximum dry density ρ_{dmax} and optimum water content $w_{opt.}$

enriched in comparison to WKA and TBKA (being similar source products) due to the hydrothermal action (Lowe and Balks 2019; Heap and Violay 2021) of RM ash falling on it. The resulting pulverization of GKA, therefore, gave it a friable and more weathered structure (thus, color change to golden) than WKA and TBKA.

A higher WIP meant a greater amount of alkalis ($Na_2O + K_2O$, which are removed later for rhyolites and dacites) remaining after weathering and therefore lesser weathering. Also, the concentration of sesquioxides ($TiO_2 + Al_2O_3 + Fe_2O_3$) for all chemical components (CWI) was highest for PB and lowest for WKA. In other words, this also meant lesser loss of SiO_2 from the WKA sample and, therefore, least weathering in comparison to PB and remaining tephra samples. By using WIP and CWI as such, the effect of both alkalis and sesquioxides was taken into consideration.

All of these factors lead to higher breakage values for more weathered GKA, RM, and MA samples in comparison to TBKA, WKA, and PB samples which were less weathered and identical individually in bulk mineralogical aspect. These trends presented in terms of weathering state (evaluated by WIP and CWI) against breakage (computed by the Hardin, and Miura and Yagi indices) values (Fig. 16) showed identical orders. The comparatively lower breakage for

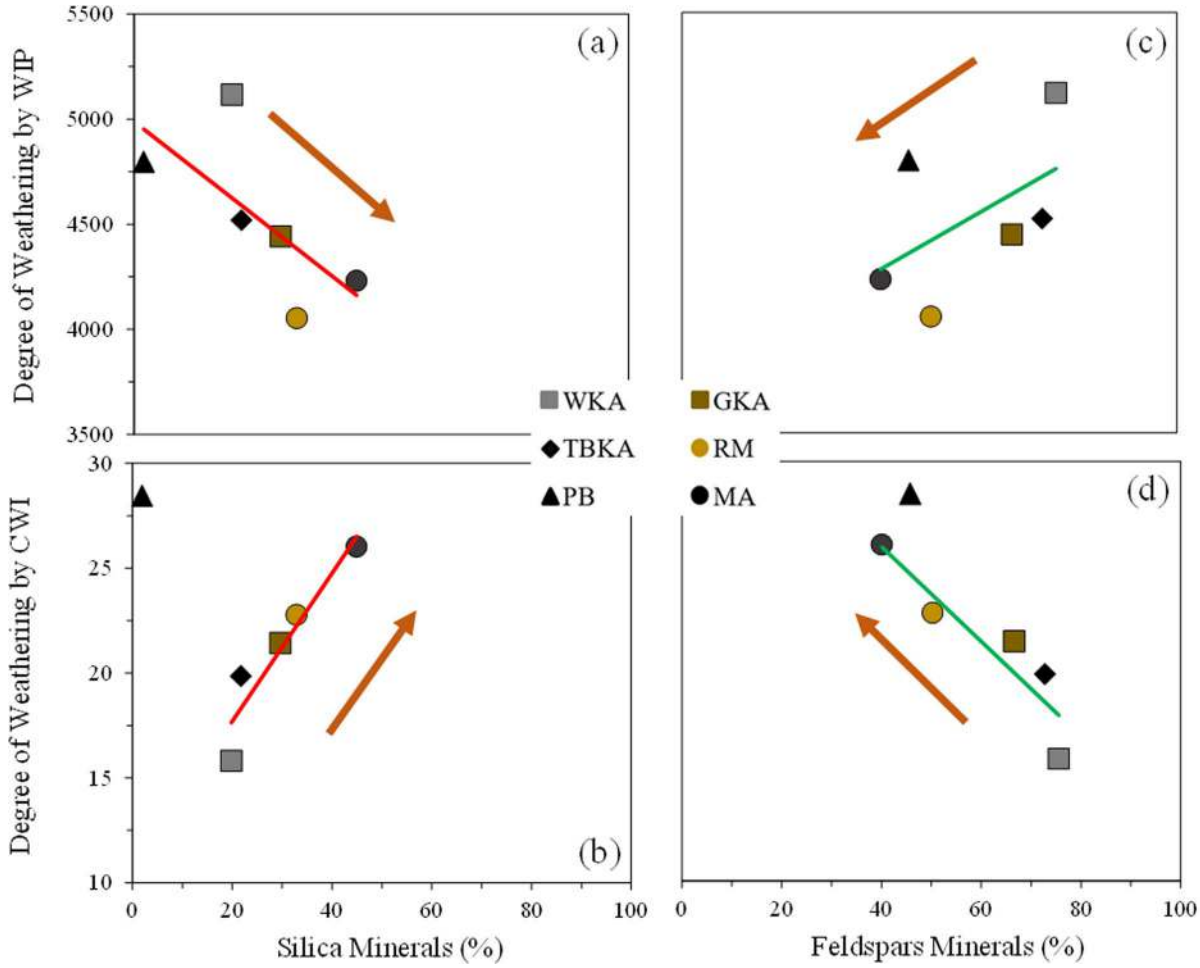

Fig. 15 Weathering state in terms of WIP and CWI against Silica and Feldspar minerals (arrows indicate weathering progression)

uniformly-graded PB in comparison to the remaining tephras could be attributed to the presence of heavier minerals such as augite and forsterite, thus making particles extremely hard and leading to an increase in their G_s.

As such, considering the different geological origins of the studied tephras, the physio–chemical and compaction parameters were interlinked and seemed to be interdependent. Different weathering tendencies and mineralogical abundancies were found to control the geotechnical properties such as compaction parameters (ρ_{dmax} and w_{opt}.) and post-compaction breakage.

Furthermore, to highlight the effect of physical and chemical parameters on the geotechnical characteristics, the variation in shear strength of the compacted tephras ($D_c \approx 90\%$) was studied (Sood et al. 2022b). It was found that the shear strength of the tephras differed with the resultant particle sizing, weathering state, and mineralogy of the deposits. As shown in Fig. 17, for the monotonic triaxial shear tests carried under drained '*D*' and undrained '*U*' conditions, the effective stress paths *q* versus *p*' became asymptotic to the failure line. The failure line or gradient of these stress paths, *M*, was correlated to the interparticle friction angle φ using the following equation:

$$M = q/p' = (6\sin\varphi)/(3 - \sin\varphi) \quad (2)$$

For the range of confining pressures 50–200 kPa studied, the φ of WKA tephra (41.5°) was higher

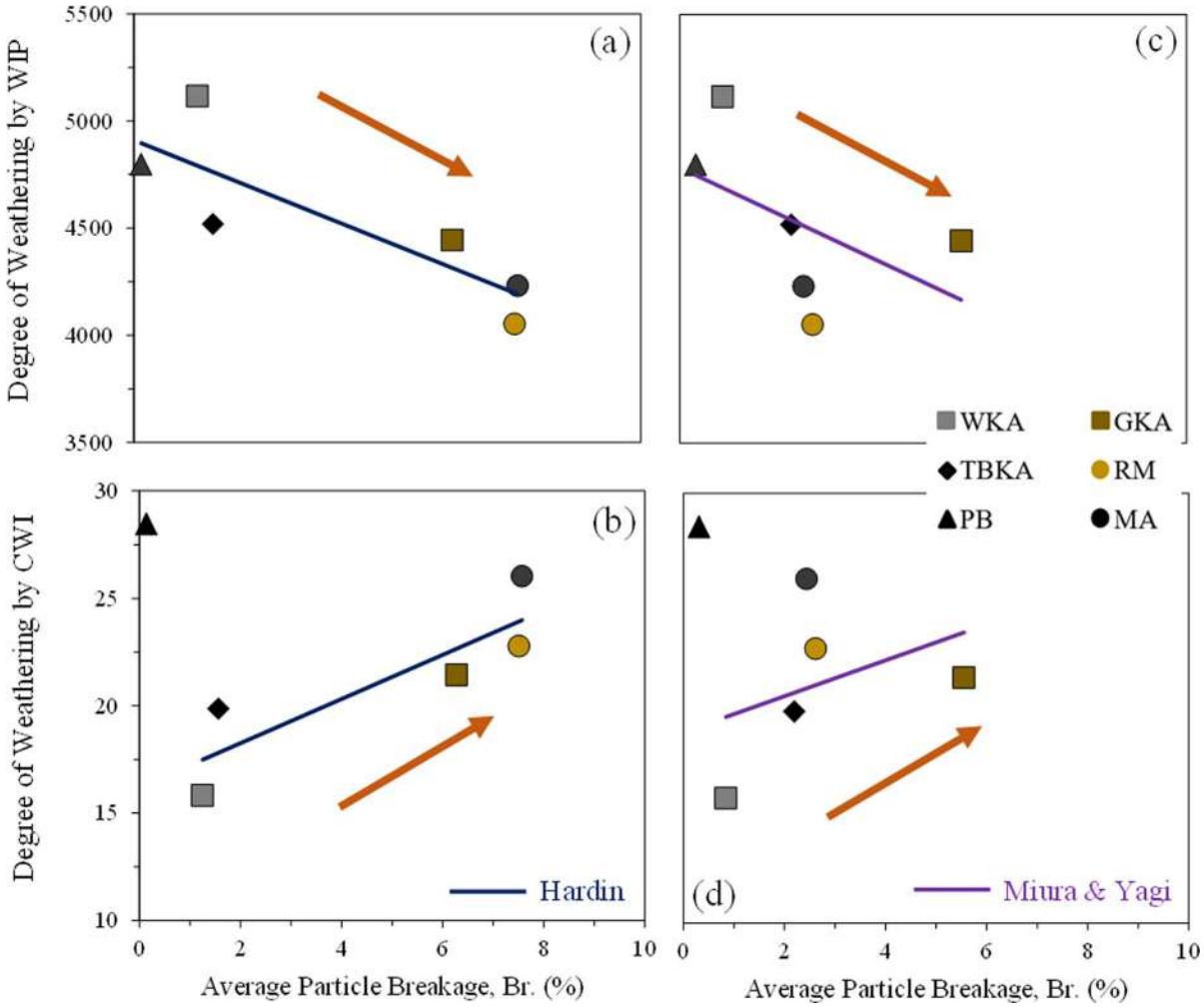

Fig. 16 Weathering state and associated particles breakages in terms of Hardin (1985) and Miura and Yagi (1997) indices (arrows indicate weathering progression)

than that of GKA (35.7°) and MA (35.5°) tephras (Heap and Violay 2021). This was due to the granular and least weathered nature of WKA, also leading to a higher resistance among the studied tephras.

In accordance, the highest post shear breakage Br. or lowest friction angle φ for basalt andesitic MA in comparison to the other tephras, was as a result of its highest weathering state as detected from its lowest WIP value (Fig. 18). This was relatively eventuated through the highest amounts of feldspars in MA, with higher silica accountable due to lithics intermixing. Thus, the chemical composition seemed to affect the shear strength of the studied tephras.

6 Conclusions

As such, in this study, eleven tephra samples (basalt to rhyolitic) collected from the North Island of New Zealand were investigated to characterize their physical (grain size, specific gravity, and morphology), chemical (elemental and mineralogy using X-ray fluorescence and X-ray diffraction) and compaction characteristics (maximum dry density, optimum water content, and particle breakage). The following conclusions were accordingly drawn.

i. Depending on the geology of the sites and weathering induced, the tephras presented con-

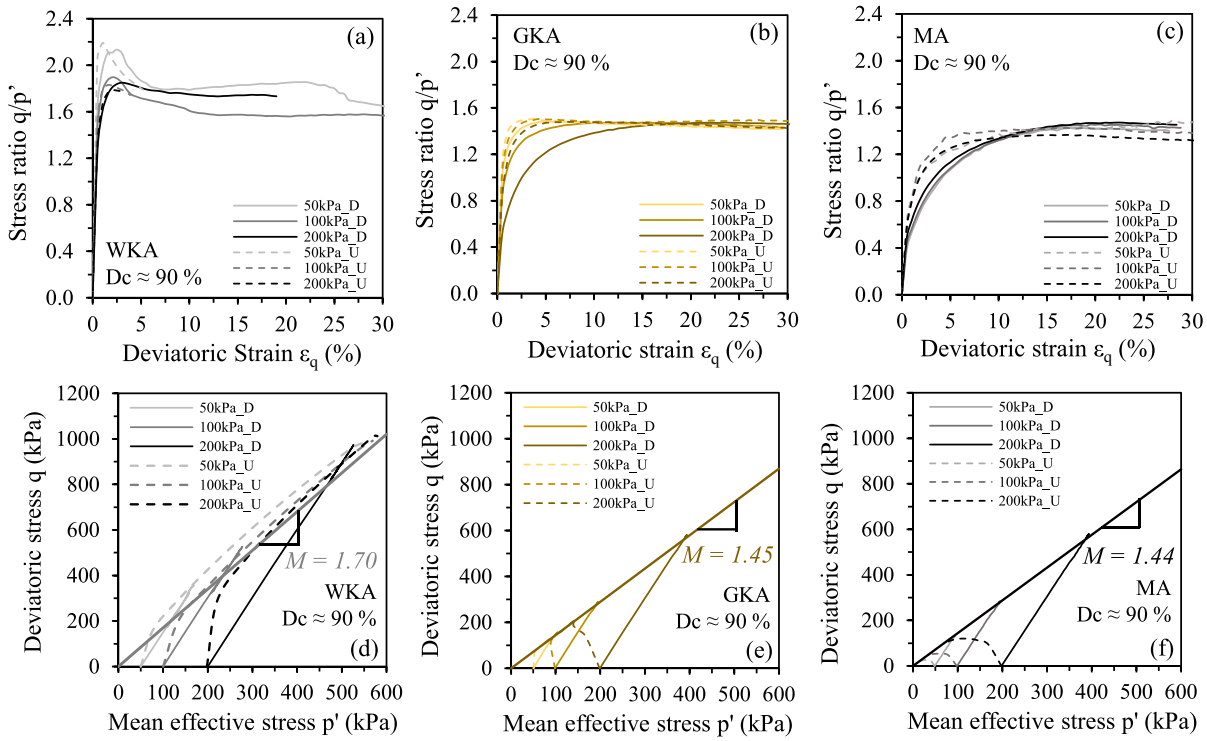

Fig. 17 Stress ratios q/p' versus ε_q and stress paths q versus p' curves for the tephras WKA, GKA and MA under monotonic triaxial conditions (Sood et al. 2022b)

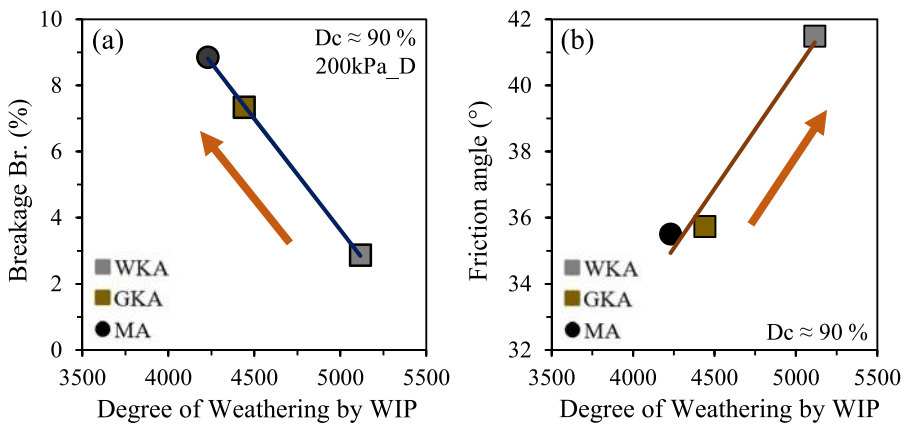

Fig. 18 Geotechnical parameters such as post shear breakage Br. and friction angle related to weathering index WIP (arrows indicate weathering progression, Sood et al. 2022b)

siderable differences in their physical and chemical properties. The samples included a wide range of particle sizes from gravel, sand, and silt to slight clay and chemical variability from basalts to rhyolites. For certain Rotorua deposits such as those collected from close proximities between Tarawera basaltic and Kaharoa rhyolitic depositions (TBKA, TB, and BPA), admixing was evident in deviations from their specific gravity (G_s) values. Thus, in addition to checking the density of a natural volcanic deposit, G_s was also used for checking intermixing.

ii. The elemental oxides and mineralogical compositions were used as the primary indicators to assess the weathering state of the tephra deposits. The major oxides expressed in terms of

weathering indices such as WIP, CWI, and A–CN–K plots, and minerals assemblages (quartz–feldspar balancing) in Q–A–P plots along with depositional settings were used to properly evaluate the weathering state.

iii. All of them being slightly weathered enabled their utilization as potential backfilling geomaterials for engineering applications. The applicability of these tephras for backfilling was further checked by compaction tests. The well-graded tephras with non-plastic fines (WKA, TBKA, and GKA) and fine-grained tephras (MA and RM) with plastic fines showcased better compaction properties than uniformly graded PB tephra with no fines content.

iv. The post-compaction breakage values fell below 10%, therefore, encouraging the use of these deposits as structural fills. The higher post-compaction breakage of fine-grained tephras than well-grained and uniformly-grained tephras was accountable to factors such as deposition, intermixing, and current weathering state. The test results also confirmed that the higher degree of weathering led to higher particle breakage. Yet, the degree of weathering and, thus the associated particle breakage, was inevitably linked to the quartz and feldspar contents. It was seen that more weathered volcanic deposits such as RM and MA, having enriched silica (quartz) content and/or low feldspars content due to their mode of deposition (base surge) and intermixing, showed higher particle breakage in comparison to the other deposits. The GKA deposit, also showcased higher breakage, in response to pulverization and intermixing by falling ash and countryside lithics.

v. The quantification of the weathering state using chemical weathering indices and mineralogical compositions (silica–feldspar balancing), therefore, had a measurable impact on ground investigation practices. This approach enabled the interpretation of different tephra profiles as well as their effects on engineering properties such as compactability, breakage, and shear strength.

Nevertheless, before the use of compacted tephras as structural fills can be further recommended, it is of paramount importance to understand their response when subjected to extreme rain and flood events due to climate change, and associated potential accelerated weathering processes in combination with earthquake conditions. But firstly it was important to distinguish different tephra types on the fundamental basis of their physical and chemical properties, as achieved in this paper. To proceed further, complementary and detailed laboratory investigations of their geotechnical engineering properties (strength, compressibility, collapsibility, liquefaction potential, etc.) have been conducted by the authors, the results of which will be available in the forthcoming papers.

Acknowledgements All the tests were conducted at University of Canterbury, Christchurch, New Zealand. The authors would like to thank Mr. Siale Faitotonu, Dr. Ali Tasalloti and Dr. Sean Rees for their valuable help in the Geomechanics laboratory. We would also like to thank Mr. Shaun Mucalo who helped with SEM testing and Dr. Vineet Shah for his valuable guidance on XRD testing. We also wish to acknowledge the financial support provided by Dept. of Civil and Natural Resources Engineering and Dept. of Science at the University of Canterbury, DEVORA and QuakeCoRE.

Funding Open Access funding enabled and organized by CAUL and its Member Institutions.

Data availability Enquiries about data availability should be directed to the authors.

Declarations

Conflict of interest The authors have not disclosed any competing interests.

Open Access This article is licensed under a Creative Commons Attribution 4.0 International License, which permits use, sharing, adaptation, distribution and reproduction in any medium or format, as long as you give appropriate credit to the original author(s) and the source, provide a link to the Creative Commons licence, and indicate if changes were made. The images or other third party material in this article are included in the article's Creative Commons licence, unless indicated otherwise in a credit line to the material. If material is not included in the article's Creative Commons licence and your intended use is not permitted by statutory regulation or exceeds the permitted use, you will need to obtain permission directly from the copyright holder. To view a copy of this licence, visit http://creativecommons.org/licenses/by/4.0/.

References

ASTM D698 (2012) Standard test methods for laboratory compaction characteristics of soil using standard effort (12,400 ft-lbf/ft^3 (600 kN-m/m^3)), ASTM International, West Conshohocken, PA

ASTM D854 (2014) Standard test methods for specific gravity of soil solids by water pycnometer, ASTM International, West Conshohocken, PA.

ASTM D2487 (2017a) Standard practice for classification of soils for engineering purposes (Unified Soil Classification System), ASTM International, West Conshohocken, PA

ASTM D7928 (2017b) Standard test method for particle-size distribution (gradation) of fine-grained soils using the sedimentation (hydrometer) analysis, ASTM International, West Conshohocken, PA

ASTM D4318 (2017c) Standard test methods for liquid limit, plastic limit, and plasticity index of soils. ASTM International, West Conshohocken, PA

Aldeeky H, Al Hattamleh O (2018) Prediction of engineering properties of basalt rock in Jordan using ultrasonic pulse velocity test. Geotech Geol Eng 36:3511–3525. https://doi.org/10.1007/s10706-018-0551-6

Agustín-Flores J, Nemeth K, Cronin SJ, Lindsay J, Kereszturi G, Brand BD, Smith IEM (2014) Phreatomagmatic eruptions through unconsolidated coastal plain sequences, Maungataketake, Auckland Volcanic Field (New Zealand). J Volcanol Geothermal Res 276:46–63. https://doi.org/10.1016/j.jvolgeores.2014.02.021

Bowen NL (1928) The evolution of the igneous rocks. Princeton University Press, Princeton, p 332

Brown SJA, Smith RT, Cole JW, Houghton BF (1994) Compositional and textural characteristics of the strombolian and surtseyan K-Trig basalts, Taupo Volcanic Centre, New Zealand: implications for eruption dynamics. NZ J Geol Geophys 37:113–126. https://doi.org/10.1080/00288306.1994.9514604

Cecconi M, Scarapazzi M, Viggiani GMB (2010) On the geology and the geotechnical properties of pyroclastic flow deposits of the Colli Albani. Bull Eng Geol Environ 69:185–206. https://doi.org/10.1007/s10064-009-0250-x

Ewart A, Cole J (1967) Textural and mineralogical significance of the Granitic Xenoliths from the Central Volcanic Region, North Island, New Zealand. NZ J Geol Geophys 10:31–54. https://doi.org/10.1080/00288306.1967.10428183

Fedo CM, Nesbitt HW, Young GM (1995) Unraveling the effects of potassium metasomatism in sedimentary rocks and paleosols, with implications for paleoweathering conditions and provenance. Geology 23:921–924. https://doi.org/10.1130/0091-7613(1995)023%3c0921:UTEOPM%3e2.3.CO;2

Fiantis D, Nelson M, Shamshuddin J, Goh TB, Van Ranst E (2010) Determination of the geochemical weathering indices and trace elements content of new volcanic ash deposits from Mt. Talang (West Sumatra) Indonesia. Eurasian Soil Sci 43:1477–1485. https://doi.org/10.1134/S1064229310130077

Fontoura TB, Coutinho RQ, da Silva FOT (2023) Geochemical and mineralogical contributions in the study of sedimentary rock (Barreiras Formation) soils, Recife/Brazil: implications for landslides. Geotech Geol Eng 41:205–224. https://doi.org/10.1007/s10706-022-02274-8

Francisca FM, Bogado GO (2019) Weathering effect on the small strains elastic properties of a residual soil. Geotech Geol Eng 37:4031–4041. https://doi.org/10.1007/s10706-019-00891-4

Goldich SS (1938) A study in rock-weathering. J Geol 46(1):17–58

Gobin M, Yasufuku N, Liu G, Watanabe M, Ishikura R (2023) Small strain stiffness, microstructure and other characteristics of an allophanic volcanic ash. Eng Geol 313:106967. https://doi.org/10.1016/j.enggeo.2022.106967

Hardin BO (1985) Crushing of soil particles. J Geotech Eng 111(10):1177–1192. https://doi.org/10.1061/(ASCE)0733-9410(1985)111:10(1177)

Harnois L (1988) The CIW index: a new chemical index of weathering. Sediment Geol 55:319–322. https://doi.org/10.1016/0037-0738(88)90137-6

Hatheway AW (2009) The complete ISRM suggested methods for rock characterization, testing and monitoring 1974–2006. Environ Eng Geosci 15(1):47–48. https://doi.org/10.2113/gseegeosci.15.1.47

Hayes J, Wilson TM, Deligne NI, Cole J, Hughes M (2017) A model to assess tephra clean-up requirements in urban environments. J Appl Volcanol. https://doi.org/10.1186/s13617-016-0052-3

Heap MJ, Violay ME (2021) The mechanical behaviour and failure modes of volcanic rocks: a review. Bull Volcanol 83:33. https://doi.org/10.1007/s00445-021-01447-2

Hiess J, Cole JW, Spinks KD (2007) Influence of the crust and crustal structure on the location and composition of high-alumina basalts of the Taupo Volcanic Zone, New Zealand. NZ J Geol Geophys 50(4):327–342. https://doi.org/10.1080/00288300709509840

Lee PY, Suedkamp RJ (1972) Characteristics of irregularly shaped compaction curves of soils. Highw Res Rec 381:1–9

Leonard G, Cole JW, Nairn IA, Self S (2002) Basalt triggering of the c. AD 1305 Kaharoa rhyolite eruption, Tarawera Volcanic Complex, New Zealand. J Volcanol Geothermal Res 115:461–486. https://doi.org/10.1016/S0377-0273(01)00326-2

Lindsay JM, Leonard GS, Smid ER, Hayward BW (2011) Age of the Auckland Volcanic field: a review of existing data. NZ J Geol Geophys 54(4):379–401. https://doi.org/10.1080/00288306.2011.595805

Liu H, Wang C, Wu D, Liu X, Zhang Z (2022) Deformation and critical dynamic stress for compacted volcanic ash subjected to monotonic and dynamic loads. Constr Build Mater 358:129454. https://doi.org/10.1016/j.conbuildmat.2022.129454

Lowe DJ (1990) Tephra studies in New Zealand: and historical overview. J R Soc NZ 20(1):119–150. https://doi.org/10.1080/03036758.1990.10426736

Lowe DJ, Balks MR (2019) Introduction to tephra-derived soils and farming, Waikato-Bay of Plenty, North Island, New Zealand. University of Wisconsin-Platteville Education Abroad Program: Winterim Field Trip (15-17 January, 2019). School of Science (Earth Sciences), University of Waikato, Hamilton, p 82

Miura S, Yagi K (1997) Particle breakage of volcanic coarse-grained soils and its evaluation. Proc Jpn Soc Civ Eng 561/III-38: 257−269. https://doi.org/10.2208/jscej.1997.561_257 (in Japanese)

Menendez OH, Lopes BDCFL, Caicedo B, Neto MPC (2022) Microscopic and mineralogical characteristics behind the

engineering properties of a compacted andesitic volcanic soil. J S Am Earth Sci 115:103752. https://doi.org/10.1016/j.jsames.2022.103752

Nairn IA (1979) Rotomahana-Waimangu eruption, 1886: base surge and basalt magma. NZ J Geol Geophys 22:363–378. https://doi.org/10.1080/00288306.1979.10424105

Nairn IA, Shane PR, Cole JW, Leonard GJ, Self S, Pearson N (2004) Rhyolite magma processes of the ~AD 1315 Kaharoa eruption episode, Tarawera volcano. New Zealand J Volcanol Geotherm Res 131(3–4):265–294. https://doi.org/10.1016/S0377-0273(03)00381-0

Nesbitt HW, Young GM (1982) Early proterozoic climates and plate motions inferred from major element chemistry of lutites. Nature 299(5885):715–717. https://doi.org/10.1038/299715a0

Nesbitt H, Fedo C, Young G (1997) Quartz and Feldspar stability, steady and non-steady-state weathering, and petrogenesis of siliciclastic sands and muds. J Geol 105:173–191. https://doi.org/10.1086/515908

Parker A (1970) An index of weathering for silicate rocks. Geol Mag 107(6):501–504. https://doi.org/10.1017/S0016756800058581

Price JR, Velbel MA (2003) Chemical weathering indices applied to weathering 518 profiles developed on heterogeneous felsic metamorphic parent rocks. Chem Geol 202(3–4):397–416. https://doi.org/10.1016/j.chemgeo.2002.11.001

Rendón MI, Viviescas JC, Osorio JP, Hernandez MS (2020) Chemical, mineralogical and geotechnical index properties characterization of volcanic ash soils. Geotech Geol Eng 38:3231–3244. https://doi.org/10.1007/s10706-020-01219-3

Rijkse W (1974) Definition: boundaries between yellow-brown pumice soils and related or associated soils. In: Soils Groups of New Zealand, Part 1. Yellow-brown pumice soils. Read NE (Ed.). NZ Soc Soil Sci Wellington, p 251

Ruxton BP (1968) Measures of the degree of chemical weathering of rocks. J Geol 76:518–527

Searle EJ (1961) The petrology of the Auckland basalts. NZ J Geol Geophys 4(2):165–204. https://doi.org/10.1080/00288306.1961.10423136

Schellmann W (1981) Considerations on the definition and classification of laterites. In: Proceedings of the International Seminar Lateritisation Processes, Trivandrum, India, pp 1−10

Sood S, Chiaro G, Wilson T, Stringer M (2022a) Comparison of small-strain shear modulus of beach and volcanic sands. In: Sitharam TG, Kolathayar S, Jakka R (Eds) Earthquake Geotechnics. Lect Notes Civ Eng, vol 187, pp 271–281. https://doi.org/10.1007/978-981-16-5669-9_23

Sood S, Chiaro G, Wilson T, Stringer M (2022b) Monotonic drained and undrained shear strength behaviour of compacted weathered airfall tephras. In: Proc Indian Geotech Conf, GEOLEAP, Kochi, India, p 12

Souri B, Watanabe M, Sakagami K (2006) Contribution of Parker and product indexes to evaluate weathering condition of Yellow Brown Forest soils in Japan. Geoderma 130(3–4):346–355. https://doi.org/10.1016/j.geoderma.2005.02.007

Stringer ME (2019) Separation of pumice from soil mixtures. Soils Found 59(4):1073–1084. https://doi.org/10.1016/j.sandf.2019.05.004

Sueoka T (1988) Identification and classification of granite residual soils using chemical weathering index. In: Proceedings of the 2nd international conference on geomechanics in tropical soils, Singapore, pp 55−61

Torabi-Kaveh M, Rizi FS, Tajbakhsh G, Khodami M, Menendez B (2023) The use of chemical and textural indices to predict geotechnical properties of granites with different degrees of weathering. Bull Eng Geol Environ 82:362. https://doi.org/10.1007/s10064-023-03387-x

Vidana Pathiranagei S, Gratchev I, Cui C, Elsmore B (2023) New weathering classification system of rocks based on the engineering properties. Bull Eng Geol Environ 82:60. https://doi.org/10.1007/s10064-023-03071-0

Wesley LD (2001) Determination of specific gravity and void ratio of pumice materials. Geotech Test J 24:418–422. https://doi.org/10.1520/GTJ11139J

Yamada I (1988) Tephra as parent material. In Proceedings of the 9th international soil classification workshop, Japan (Kinloch DI, Shoji S, Beinroth FH, Eswaran H, Eds.), pp 509−519

Publisher's Note Springer Nature remains neutral with regard to jurisdictional claims in published maps and institutional affiliations.